Institute of Aerospace Systems

RWTH AACHEN UNIVERSITY

DLR Design Challenge 2025

MedEvac Aircraft

ASCLERA

Project team

Joshua Hector
Timon Helmich
Felix Loick
Ty Pruschke
Justus Trost
Jan Weisgerber

Academic Support and Advisors

Univ.-Prof. Dr.-Ing. Eike Stumpf

Ansgar Kirste, M.Sc.

Submitted on July 21, 2025

Team Members

Joshua Hector
Mechanical Engineering B.Sc.
6th Semester

Timon Helmich B.Sc.
Aerospace Engineering M.Sc.
3rd Semester

Felix Loick
Mechanical Engineering B.Sc.
7th Semester

Ty Pruschke B.Sc.
Business Administration and Engineering: Mechanical Engineering M.Sc.
3rd Semester

Justus Trost
Mechanical Engineering B.Sc.
10th Semester

Jan Weisgerber B.Sc.
Aerospace Engineering M.Sc.
2nd Semester

Institute of Aerospace Systems

RWTH AACHEN UNIVERSITY

Univ.-Prof. Dr.-Ing.
Eike Stumpf

Wuellnerstrasse 7
52062 Aachen
GERMANY
Phone: +49 241 80-96800

stumpf@ilr.rwth-aachen.de

Institute of Aerospace Systems | Wuellnerstrasse 7, 52062 Aachen 415310

21.07.2025

Confirmation for submission

The hereby submitted project work has been confirmed by the Head of Institute of Aerospace Systems (ILR) and is endorsed for the submission in the DLR Design Challenge 2025. The work has been done independently from currently enrolled students from RWTH Aachen University without further assistance of our institute.

i.A.

ILR | RWTH AACHEN UNIVERSITY
Institut für Luft- und Raumfahrtsysteme
Univ.-Prof. Dr.-Ing. Eike Stumpf
Wüllnerstraße 7
52062 Aachen | GERMANY

Univ.-Prof. Dr.-Ing. Eike Stumpf

Abstract

ASCLERA is a short/medium range medical evacuation and air ambulance aircraft capable of transporting up to 15 patients over a range of 2,500 km. This report outlines the design process of the aircraft in detail. This includes choosing a suitable configuration, initial sizing as well as a detailed design loop. During the design process, versatility, performance and technical simplicity are focused on. The design loop is implemented by using a MATLAB script linking the aerodynamics analytics tool calculatePolar and a preliminary design tool, iterating until the value for the maximum take-off mass converges. The final mass is estimated to be 11,703 kg. A high performance twin turboprop aircraft with an oscillating advanced dropped hinged flap is designed. An advanced flight control system including flight envelope protections and gust load alleviation technology maximizes patient comfort during flight phases and allows for medical procedures to be carried out during flight. The design is able to operate on short runways at a high altitude in mountainous terrain while maintaining high levels of reliability.

The cabin design focuses on modularity and rapid configurability. The fuselage of the aircraft is elliptic, increasing usable cabin space. The two door configuration allows simultaneous boarding of both high acuity and low acuity patients, reducing the turnaround time significantly. A state of the art loading system using rails allows a variety of modularized equipment to be loaded in minimal time, enabling the simultaneous transport of patients of varying acuity levels and reducing the response time compared to current aircraft.

Zusammenfassung

ASCLERA ist ein medizinisches Evakuierungs- und Luftrettungsflugzeug für kurze bis mittlere Strecken, das bis zu 15 Patienten über eine Reichweite von 2,500 km transportieren kann. Dieser Bericht beschreibt den Konstruktionsprozess des Flugzeugs im Detail. Dazu gehören die Auswahl einer geeigneten Konfiguration, die anfängliche Dimensionierung sowie der Detailentwurf. Während des Entwurfsprozesses stehen Vielseitigkeit, Flugleistung und technische Einfachheit im Mittelpunkt. Der Designzyklus wird mithilfe eines Matlab-Skripts implementiert, welches das Aerodynamikberechnungsprogramm calculatePolar und das Entwurfs- Programm miteinander verbindet und so lange iteriert, bis der Wert für die maximale Startmasse konvergiert. Die endgültige Masse wird auf 11,703 kg geschätzt. Es wird ein leistungsstarkes zweimotoriges Turboprop-Flugzeug mit einem oszillierenden, multifunktionalen Hochauftriebssystem entworfen. Adaptive Regelungssysteme und intelligente Böenlastminderungstechnologie maximieren den Komfort für die Patienten während der Flugphasen und ermöglichen die Durchführung medizinischer Eingriffe während des Fluges. Das Design ermöglicht den Betrieb auf kurzen Landebahnen in hohem Gelände bei gleichzeitig hoher Zuverlässigkeit.

Die Kabine zeichnet sich durch Modularität und schnelle Konfigurierbarkeit aus. Der Rumpf des Flugzeugs ist oval, wodurch der nutzbare Kabinenraum vergrößert wird. Die Konfiguration mit zwei Türen ermöglicht das gleichzeitige Einladen von schwer- und leicht verletzten Patienten, wodurch die Durchlaufzeit erheblich verkürzt wird. Ein hochmodernes Schienenverladesystem ermöglicht das Verladen einer Vielzahl von Geräten und Sitzmöglichkeiten in kürzester Zeit, wodurch verschiedene Kombinationen an Verletzten gleichzeitig transportiert werden können und die Reaktionszeit im Vergleich zu aktuellen Flugzeugen verkürzt wird.

Contents

List of Figures

List of Tables

List of Symbols

General Symbols

b	[m]	Span
C	[–]	Coefficient
c	[m]	Chord length
D	[N]	Drag
EM	[kg]	Empty Mass
FL	[hft]	Flight Level
g	[m/s^2]	Gravitational acceleration
k	[–]	Amount
L	[N]	Lift
(L/D)	[–]	Lift-to-Drag ratio
LFL	[m]	Landing field length
m	[kg]	Mass
Ma	[–]	Mach number
MAC	[m]	Mean aerodynamic chord
MTOM	[kg]	Maximum Take-Off Mass
MZFM	[kg]	Maximum Zero Fuel Mass
n	[–]	Load factor
OEM	[kg]	Operating Empty Mass
p	[°/s]	Roll rate
P	[W]	Power
PSFC	[g/Ws]	Power Specific Fuel Consumption
(P/W)	[W/N]	Power-to-Weight ratio
q	[°/s]	Pitch rate
R	[J/kgK]	Specific gas constant of air
r	[m]	Moment arm
Re	[–]	Reynolds number
S	[m^2]	Surface area
s	[m]	Distance
SM	[%]	Static margin
T	[K]	Temperature

t	[m]	Airfoil thickness
TOFL	[m]	Take-off field length
v	[–]	Volumetric coefficient
V	[m/s]	Velocity
W	[N]	Gravitational force
(W/S)	[kg/m^2]	Wing loading
x	[m]	Position along the longitudinal axist

Greek Symbols

α	[°]	Angle of Attack
β	[°]	Slip angle
Δ	[–]	Difference
γ	[–]	Factor
κ	[–]	Isentropic expansion factor of air
Λ	[–]	Aspect ratio
λ	[–]	Taper ration
Φ	[°]	Bank angle
ρ	[kg/m^3]	Air Density
Θ	[°]	Pitch angle

Subscripts

1	Decision
AC	Aerodynamic center
additional	Additional
blade	Blade of the Propeller
CG	Center of gravity
cruise	Cruise operating point
dep	Departure airport
down	Nose down
engine	Engine
$flap$	Flap
HTP	Horizontal tailplane
ind	Induced

$initial$	Initial sizing value
L	Lift
$landing$	Landing
M	Pitching moment
$M1$	Mission 1
$M2$	Mission 2
$M3$	Mission 3
max	Maximum value
n	Iteration step
opt	Optimal
$prop$	Propeller
$prot$	Protection
ref	Reference
$rubber$	Rubber engine
$safety$	Safety
Sea	Sea level
$shaft$	Engine shaft
T/O	Take-off
$taxi$	Taxiing
TF	Trip Fuel
$total$	Total
up	Nose up
$visc$	Viscous
VTP	Vertical tailplane
W	Wing
wav	Wave
z	Downwards facing aircraft fixed axis

Abbrevations

3D	Three dimensional
AC	Aerodynamic center
ADAC	Allgemeiner Deutscher Automobilclub
AGV	Automated guided vehicle

AI	Artificial Intelligence
APU	Auxiliary power unit
ASCLERA	Aeromedical System for Configurable Life-saving Evacuation and Rapid Aid
ASL	Above sea level
ATC	Air traffic control
BWB	Blended Wing Body
CFRP	Carbon-fiber-reinforced plastics
CG	Center of gravity
DIN	German Institute for Standardization
DLR	German Aerospace Center
ECMO	Extracorporeal membrane oxygenation
EC	Electrical Cardiometry
EIS	Entry Into Service
EIT	Electrical Impedance Tomography
eVTOL	Electric vertical take-off and landing
FEP	Flight envelope protections
FPFM	Flight Planning and Fuel Management
GSE	Ground support equipment
HTP	Horizontal tailplane
ICAO	International Civil Aviation
ISA	International Standard Atmosphere
KTW	Patient transport ambulance
MATLAB	Matrix Laboratory
MedEvac	Medical Evacuation
MFFD	Multi Function Fuselage Demonstrator
N-KTW	Emergency ambulance
NASA	National Aeronautics and Space Administration
OEI	One Engine Inoperative
POCUS	Point-of-Care Ultrasound
POC	Point-of-Care
PTU	Patient Transport Unit
REBOA	Resuscitative Endovascular Balloon Occlusion of the Aorta
RKN	Rhein-Kreis Neuss

RTW	Mobile intensive cate unit
SAF	Sustainable Aviation Fuel
SK1	High acuity
SK2	Medium acuity
SK3	Low acuity
SK	Triage categories
STOL	Short Take-Off and Landing
T/O	Take-off
TLAR	Top Level Aircraft Requirement
TOC	Top of climb
TOD	Top of descent
TRL	Technology Readyness Level
UNICADO	University Conceptual Aircraft Design and Optimization
VTP	Vertical tailplane

1 Introduction and Background

The focus of this report is the design of an aircraft that is capable of transporting up to 15 patients over a mission radius of 1,250 km while maintaining a short take-off and landing distance required on short runways in remote locations. The proposed solution in this report, ASCLERA (Aeromedical System for Configurable Life-saving Evacuation and Rapid Aid, originating from the Greek God for healing, Asclepius), aims to combine versatility, patient comfort, and response time to be feasible in a wide variety of medical evacuation missions. The following report describes the aircraft design process and the resulting design in detail. First, the history of medical evacuation and current aircraft in use are introduced. Next, relevant literature is discussed in section 2. The first steps of the design process, choosing a configuration and setting an initial sizing point, are presented in section 3 . The design loop is explained in section 4. A detailed description of all aircraft features can be found in section 5. An analysis of the task missions is carried out in section 6. Finally, the results of the report are discussed in section 7.

1.1 History of MedEvac

Since its invention, Aero Medical Evacuation (MedEvac) has increased the likelihood of survival of patients in remote locations substantially. MedEvac aviation can be grouped into two different types: Long Range Evacuation with fixed wing aircraft and short range missions with rotorcrafts [17]. While fixed wing aircraft have a much higher cruising speed and range than helicopters, they are limited in their use due to their need for a runway and an airport to operate. Helicopters can land in much smaller and difficult to access areas and are therefore mainly used in Air Ambulance missions today. However, in more remote locations, proper hospitals are often hundreds of kilometers away, making the use of rotorcrafts impractical.

The first recorded evacuation of a wounded soldier by plane occurred in 1917, when a British soldier was evacuated from the Sinai desert using a DH-4 biplane. The soldier was sitting in the observer seat, and the journey took only 45 minutes instead of multiple days by foot [24]. During World War 2, larger dedicated transport aircraft and specially trained flight nurses were deployed to evacuate wounded soldiers from European battlefields [58]. Civilian MedEvac only became widespread in the 1960s, when the boom of the automotive industry and the resulting rise in vehicle traffic accidents required new ways to transport injured patients to hospitals quickly from locations potentially further away from hospitals or difficult to access. At this time a more organized approach to trauma treatment was also developed [58]. In 1973, as mediterranean tourism boomed and medical emergencies abroad rose, the "Allgemeiner Deutscher Automobilclub" (ADAC) organized its first long range MedEvac service in Germany, transporting German patients from abroad back home to Germany [1]. Initially, the ADAC chartered planes and converted these for MedEvac flights individually. Later, a dedicated fleet was established to fly long-range missions. Today, the MedEvac service transports patients from all over the world back to Germany, including a flight from Hawaii in 1997 [1].

1.2 Current MedEvac Aircraft in use

Today, short range patient transport flights within Germany are carried out using Airbus H145 and H135 Helicopters by the ADAC [3] and DRF [28] Luftrettung. Longer range MedEvac flights to transport patients in need of critical care back to Germany are also carried out by the ADAC. Dornier Fairchild 328-Jet and Bombardier Learjet 60XR aircraft with a range of 3,700 km and 3,800 km respectively are used currently. Both planes are equipped with mobile heart-lung machines and are pressurized, allowing the cabin pressure to be adapted to the patients needs [2].

The Do-328-Jet can carry up to 10 patients from short runways with a minimum runway length of 1,300 m [2]. The maximum take-off mass is 15,660 kg [26]. Furthermore, the aircraft can be equipped with a heart-lung machine or adapted for intensive infant care missions.

The Learjet 60XR is less versatile than the Do-328-Jet. The medical equipment onboard cannot be aligned with patients needs as easily due to spatial constraints. The turbofan propulsion system and the resulting higher cruising speed means it is mainly used for medium and long range missions [2].

1.3 Mission Scenarios and Top Level Aircraft Requirements

Top Level Aircraft Requirements (TLARs) are the basic requirements that a MedEvac aircraft must meet to successfully fulfill its mission - the safe and efficient transportation of patients under medical care. They define the framework for the design and operation of the aircraft including the equipment on board. The mission parameters given in the task are presented in Table 1.

Parameter	Mission 1 *Remote Response*	Mission 2 *Disaster Response*	Mission 3 *Critical Transfer*
Location			
Mission Radius	153 km	400 km	1,250 km
Ground Altitude	2,850 m	0 m	150 m
Atmosphere	ISA +20	ISA -35	ISA +5
Airfield			
Runway Length	756 m	1,250 m	1,000 m
Surface Condition	Hard turf	Icy concrete	Concrete
Friction Coefficient	0.05	0.02	0.04
Timing			
Total Mission Time	1.5 hours	3.5 hours (per trip)	9 hours
Response Time	0.5 hours	45 minutes	2 hours
Turnaround Time	10 minutes	10 minutes	25 minutes
Number of round trips	1	2	1
Payload			
Medical Personnel	2	4	2
Cargo	—	500 kg	—
Patients			
Total Injured	5	15 (per trip)	1
Condition (High)	1	0	1
Condition (Medium)	1	4	0
Condition (Low)	3	11	0

Table 1: Specifications of the missions.

The mission parameters in Table 1 establish the foundational constraints for the cabin design. Mission 2, with its high patient count, dictates the required capacity, while Mission 3, a critical care transfer, sets the standard for the highest level of medical capability. To meet these demands, the following key TLARs for the cabin were established:

- Simultaneous Multi-Acuity Care: The cabin must be able to accommodate and deliver care/treatment to multiple patients with different levels of acuity during a single flight. This requires the simultaneous accessibility to patients, availability of workspace to prepare treatments, and the availability of different accommodation types and their associated medical equipment.
- An estimated payload capacity of 3,600 kg must be achieved in order to take care of 15 patients. This also includes 6 crew members and medical equipment onboard.
- Rapid Mission Reconfigurability: The cabin layout must be modular to allow for rapid restocking during missions (Mission 1) and rapid reconfiguration between missions. This ensures the aircraft can efficiently switch from a high-density, 15-patient transport (Mission 2) to a single-patient, long-range intensive care environment (Mission 3) within the given response time.
- Cabin adaptability and patient throughput: A versatile stretcher management system is essential. Typical MedEvac helicopters such as the Airbus H145 accommodate up to two stretchered patients with accompanying medical staff [9]. Military adaptations of transport aircraft can be converted to carry 24 stretchers and seven attendants, reflecting the need for scalable cabin configurations [53].

The key TLARs for the aircraft design are as follows:

- Operational priority and ground handling integration: To ensure timely execution of MedEvac missions, the aircraft must be capable of receiving priority handling by air traffic control (ATC) and must be compatible with streamlined ground operations procedures to minimize delays at remote and urban airfields [33].
- Range and operational radius: The aircraft must be capable of covering both short- and long-range missions. A range of 2,500 km must be achieved to carry out the longest mission without refueling at the pick up location for ferry flights between peripheral facilities and central hospitals, as well as shorter missions of approximately 150 km in difficult-to-access regions.
- Short Take-Off and Landing (STOL) capabilities on unpaved runways: The aircraft must be able to take off and land on a 756 m runway at a field elevation of 2,850 m AMSL.

- A cruising altitude of 20,000 ft must be achieved.
- The cruising speed is set to Mach 0.4

A detailed explanation of the TLARs can be found in subsection 3.1.

1.4 The future of MedEvac aircraft

The evolution of MedEvac aircraft is defined by several converging technological, operational, and environmental trends. Current developments underscore the sector's transition toward faster response times, smart integration, decarbonized propulsion, and advanced mission-specific architectures.

Speed, Connectivity and Telemedicine Integration

Emerging communications technologies allow on-ground medical specialists to monitor and guide in-flight care remotely. Through secure mobile interfaces, onboard medical crews can receive real-time data and advice, improving outcomes during transit. A recent market analysis emphasizes that mobile telemedicine systems are revolutionizing onboard critical care, enabling remote equipment adjustment and collaborative decision-making [16, 93].

Modular and Adaptive Cabin Design

New cabin designs prioritize adaptability: configurations can be changed pre-flight or in-flight to suit varying patient load, equipment needs, and mission profiles. Military-led initiatives like the US Army's Future MedEvac Cabin Technical Demonstrator highlight the collaborative development between engineers and end-users, emphasizing modular, reconfigurable spaces informed by actual operational feedback [16].

AI-Powered Mission Optimization

Artificial Intelligence (AI) plays a pivotal role in predictive analytics, optimizing dispatch procedures, flight paths, and patient care protocols. Pilot studies show that AI-enhanced systems can decrease response times and improve resource allocation [69]. In medical logistics, machine learning fuels demand forecasting and vehicle positioning, further refining readiness and deployment.

Smart Materials and Structural Health

"Smart structures" equipped with embedded sensors enable real-time structural health monitoring and adjustability such as morphing wings or cabins that adapt to load conditions. These systems can reduce maintenance costs, enhance safety, and optimize performance, for example, reducing drag or noise through active shape control [96].

Future Aircraft Concepts

Hybrid platforms such as Tilt Rotor configurations (e.g. Leonardo's NGCTR) or larger electric vertical take-off and landing (eVTOL) systems may bridge the gap between helicopters and fixed-wing aircraft, offering vertical lift with faster cruise speeds and extended range [55]. These aircraft could transform MedEvac operations by improving access to urban and remote environments with minimal infrastructure.

Future generations of MedEvac aircraft will feature digitally connected cabins, AI-supported logistics, modular interior layouts, and clean energy propulsion, all operating within smart, responsive aircraft. This technological interplay will be crucial to making global medical evacuations faster, more efficient, sustainable and patient-centered.

2 Literature Review

In this section, relevant literature used during the design process of ASCLERA is introduced.

2.1 Configuration and Initial Design

The works of Liebeck [56], Thomas [87] and Hasan et al. [44] provide insight into the advantages and disadvantages of Blended Wing Body (BWB) and Flying Wing aircraft concepts. Studies by May et al. [63] and Harris [43] are used to evaluate Tilt-Rotor aircraft concepts. While Harris [43] focuses on the complete design of Tilt-Rotor aircraft, May et al. [63] describe the challenges found in the transition period between hovering and forward flight.

Hoff et al. [45] examine the use of hydrogen as an energy source for aircraft with special regards for the necessary infrastructure. Wolleswinkel et al. [97] describe the feasibility of larger electric aircraft. In their work, the authors

claim that an energy mass fraction (EM/MTOM) of 50 % can be achieved even without the use of advanced materials, making electric propulsion concepts viable even for larger aircraft with a longer design range.

The work of Raymer [75] is useful for various areas of aircraft design. Raymer describes estimations for the initial sizing, mass estimation as well as the detailed aircraft design. Raymer also describes the potential mass reduction when using composite materials in different areas of the aircraft.

2.2 Elliptic Fuselage

In contrast to the typical round fuselage, the elliptic fuselage presents a unique set of trade-offs. On the one hand, an increase in lift L can be observed, since the fuselage acts as a Lifting Body. Frolov [37] presents a method to determine the Lift increase with a given geometry. Drela [27] conducts experimental research on a so called double-bubble fuselage. The lift increase demonstrated by Drela compared to Frolov's method is higher by a factor of 1.043.

Despite a drag D increase of the fuselage, the overall drag is reduced by 2 - 4 %. This is a result of snowball effects on different components, which overcompensate the fuselage drag increase [27].

Using the approach of Boulle [14], the volume and mass penalty of an elliptical fuselage compared to one with a circular cross section can be determined. According to Raymer [75], the increased risk of flow separation at the rear end of a wide-body fuselage can be mitigated by installing vortex generators on the aft body surface, which help delay separation and reduce the associated drag.

2.3 UNICADO - calculatePolar

The University Conceptual Aircraft Design and Optimization (UNICADO) tool chain is being developed by a consortium of multiple universities in Germany. The standalone program calculatePolar can be used to compute aerodynamic coefficients of an aircraft. calculatePolar is wrapped around LIFTING_LINE 3.1, a multiple lifting line method developed by Horstmann [46] and further expanded on by the German Aerospace Center (DLR). Each LIFTING_LINE 3.1 and calculatePolar are validated by the DLR and the university consortium respectively. [57, 81, 98]

2.4 Technology Readiness Level

The Technology Readyness Level (TRL), as defined in ISO 16290 [51], categorizes the maturity of a specific technology, ranging from basic principles observed (1) to flight-proven systems (9). The concept of TRL was first introduced by NASA [60]. It is used to assess key technologies with respect to a targeted Entry Into Service (EIS) date.

3 Initial Design

In this Chapter, the Initial Design decisions and assumptions will be explained. First, different configurations are examined and the most suitable for the required mission parameters given in the task description is chosen. Next, the wing loading (W/S), Power-to-Weight ratio (P/W) and initial mass are estimated.

3.1 Mission Parameters

Before choosing a configuration, it is necessary to derive relevant mission parameters from the TLARs identified in subsection 1.3.

The payload capacity of 3,600 kg is derived from the limiting mission 2 (M2) disaster response scenario, which includes the initial delivery of 500 kg of aid supplies. The mass of the 15 patients and 6 crew members is based on a standard estimate of 80 kg per person. Each of the four SK2 patient accommodations, including their half-reclinable seats and dedicated medical support systems, is allocated a mass of 140 kg, while each of the eleven SK3 accommodations with standard seating and basic first aid supplies is allocated 65 kg. Additionally, each of the four medical personnel accounts for a 20 kg personal kit, and a reserve of 65 kg is included for mission-specific triage and redundancy equipment. These individual mass allocations for personnel, patient accommodations, and reserves collectively result in the payload capacity of 3,600 kg.

The minimum cruise altitude is determined to be 20,000 ft based on the fact that mission 1 takes place in a mountainous environment. Based on cruise altitude and known mission data (see Table 1), mission profiles are created to calculate the required cruise speeds for the missions. Figure 1 and Figure 2 show the profiles corresponding to the two most constraining scenarios, mission 1 (M1) and mission 3 (M3).

For mission 1, a cruise Mach number of $Ma = 0.43$ is necessary to adhere to the mission's time window, assuming that the full time for response and turnaround is used. For mission 3, the same considerations lead to $Ma = 0.4$. For both calculations, a time safety factor $\gamma_{safety} = 1.2$ is considered to account for possible deviations or delays. Since mission 3 features the longest range and subsequently the longest cruise time, the design cruise Mach number is chosen to be $Ma_{\text{cruise}} = 0.4$. This ensures that the aircraft is designed to be efficient based on the longest mission flown. Mission 1 is therefore flown slightly outside the design point, but the small efficiency penalty can be neglected based on the short mission duration.

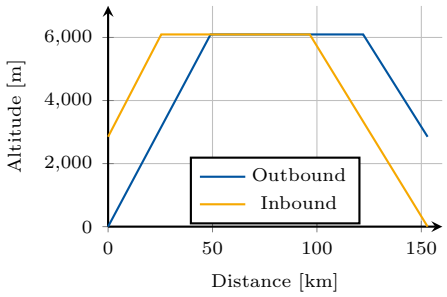

Figure 1: Profile - Mission 1.

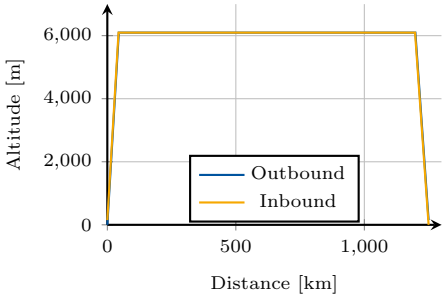

Figure 2: Profile - Mission 3.

Relevant Data	
Cruise Alt	20000 ft
Climb Rate	2500 ft/min
Descent Rate	2500 ft/min
γ_{safety}	1.2
$Ma_{cruise,M1}$	0.43
Ma_{cruise}	0.4

Table 2: Relevant data for the mission profiles.

3.2 Choosing a configuration

Choosing the correct configuration that is capable of entering into service shortly after 2035 is critical. While multiple different configurations are capable of fulfilling the requirements of the Design Challenge missions, some are more suitable than others. To choose the most suitable configuration, relevant features of the aircraft were used for a trade-off study in order to select the configuration, propulsion concept and energy source.

The most important requirements were found to be a short take-off and landing distance, the technical complexity, sustainability and the readiness of the technology. These specifications correspond to the TLARs stated in subsection 1.3, namely STOL capabilities on unpaved runways, cabin adaptability and patient throughput as well as rapid mission reconfigurability. Additionally, the risk of technical faults that lead to the grounding of the plane must be minimized. The results of this trade-off study are shown in Table 3.

Aircraft Configuration					
Concept	Payload Volume Efficiency	Aerodynamic Efficiency	STOL Capability	Technology Readiness	Result
BWB	++	++	-	-	2
Conventional	0	-	++	++	3
Conventional + Lifting Body	+	+	++	+	5
Flying Wing	+	++	--	--	-1
Propulsion Concept					
Concept	STOL Capability	Technical Complexity	System Mass	Technology Readiness	Result
Piston engine	0	+	0	++	3
Tilt-Rotor	++	-	0	0	1
Turbofan	-	-	-	++	-1
Turboprop	+	+	0	++	4
Energy Source					
Concept	Infrastructure	Environmental Impact	System Mass	Technology Readiness	Result
Electric	0	++	-	+	2
Hydrogen	-	+	-	0	-1
Kerosene	++	--	+	++	3
SAF	++	0	+	+	4

Table 3: Process used to choose the aircraft configuration, propulsion concept and energy source.

Aircraft Configuration

For the aircraft configuration, four concepts were considered. While the Blended Wing Body and the Flying Wing excel regarding aerodynamic efficiency and the useful volume of the fuselage, a more conventional configuration combines good STOL capability with well-proven technology [75]. Since one of the TLARs constrains the maximum take-off and landing distance to 756 m at an altitude of 2850 m ASL, good STOL capabilities are to be preferred here. By

extending the conventional configuration with a lifting-body fuselage, we combine the good STOL capability of the conventional design with the higher payload volume and aerodynamic efficiency of the BWB and Flying Wing. This produces the aircraft configuration of ASCLERA, examples of aircraft with similar configurations are found in [95, 27].

Propulsion Concept

In this year's Design Challenge, the aircraft is used exclusively for patient transport and medical evacuation missions. Therefore, reliability is critical, especially considering that the fleet size is most likely small and replacement aircraft are not necessarily available if the aircraft is grounded due to technical faults. Furthermore, diversions due to inflight issues can cause a complete mission failure. This makes it vital to rely on mature technology with a low level of technical complexity. While a tilt-rotor concept would be best for STOL, it is technically more complex [63, 75] and less mature than conventional piston engine and turboprop concepts. Therefore, a Tilt Rotor propulsion concept is deemed not practical for the use case. With the cruise speed being Mach 0.4, both piston and turboprop engines are more efficient than turbofan engines. Ultimately, a turboprop engine is favored over a piston engine, due to a better power-to-weight ratio and consequently better STOL capability.

Energy Source

Electric flight is enabled by carrying large batteries on board the aircraft or using a fuel cell. Carrying batteries significantly increases the aircraft mass [92] without enhancing the mission execution. While some studies show that an empty mass fraction of 50 % can be achieved in future concepts [97], it is unclear whether the necessary range can be achieved while maintaining STOL capabilities. Hydrogen as an energy source can either be used in a fuel cell to drive an electric motor, or it can be burned directly in an air-breathing engine. Storing the hydrogen, which has a significantly lower volumetric density than kerosene, requires high-pressure or low-temperature tanks, that are cylindrical [62, 88, 92]. Furthermore, current studies show that the infrastructure required for hydrogen-powered aviation will not be available in the near future [45]. Ultimately, this promotes the use of kerosene or Sustainable Aviation Fuels (SAF). Between these two energy sources, SAF should be preferred, based on their lower environmental impact, although it should be noted that environmental considerations are secondary to ensuring patient safety and comfort in MedEvac missions.

Cabin Dimensions and Patient Comfort

During the configuration selection process, further considerations were made regarding the cabin dimensions and patient comfort during transport. The cabin must have sufficient space and provide a stable environment for medical personnel to work effectively. While aerodynamically efficient, the BWB and Flying Wing configurations are not suitable for this mission, as their flight characteristics present significant challenges to patient comfort. In contrast, for a conventional configuration, the cabin design is mostly independent from the wing design, except for the wing-fuselage-intersection [90]. While the conditions during the different phases of flight may be less important for mildly injured patients, critical care patients must be treated with care during flight. Sudden movements and large forces must be avoided and a pitch angle of $\Theta = 0\ ^\circ$ should be pursued. Studies show that BWB configurations achieve an angle of attack α of approximately $3\ ^\circ$ during cruise while reaching up to $17\ ^\circ$ peak and $13\ ^\circ$ maintained angle of attack during climb [56]. This is comparatively higher than a Tube and Wing aircraft with $14\ ^\circ$ peak and $7\ ^\circ$ maintained angle of attack during climb [87].
Furthermore, due to the inability to install flaps at the trailing edge of the wing, $C_{L,max}$ would occur at a relatively high angle of attack, possibly limiting patient comfort [56]. In addition, forces and movement during rolling maneuvers inside the cabin are amplified in wider cabins [44]. This could be problematic, especially for critically injured patients, which would need to be transported in the center of the cabin to minimize movement. The Tilt-Rotor configuration does not require heavy breaking during landing or high pitch angles during take-off and initial climb. This is beneficial for patient comfort. However, Tilt-Rotor aircraft generally require larger rotors to minimize Disk Loading [43], which leads to more noise in the cabin. This can significantly decrease patient comfort especially during high power phases such as take-off and landing if no additional noise insulation is installed. Furthermore, a Power to Weight ratio of greater than 1 must be achieved for hovering flight. In combination with the complexity of the propulsion system, a mass penalty must be considered for the Tilt-Rotor configuration. Rotor downwash and subsequent vibrations can decrease patient comfort further. Another aspect that must be considered is the outwash caused by the rotors in ground proximity, which can endanger bystanders. Ultimately, this disqualifies the Tilt-Rotor configuration for the design case and the TLARs.

In contrast, the chosen configuration - a conventional layout with a lifting-body fuselage - offers inherent advantages with respect to patient comfort and operational flexibility. The conventional arrangement allows for a largely decoupled cabin geometry, enabling sufficient cabin height and flat floor designs that are essential for ergonomic patient treatment. To finalize this configuration, an elliptical cabin cross-section (width: 3.48 m, height: 2.5 m) is selected as a deliberate balance between competing geometric and systemic requirements. A lower eccentricity cross-section was rejected because its narrower floor plan would hinder simultaneous access to patients, necessitating a longer and less efficient fuselage. Conversely, a shape with higher eccentricity was also disregarded; while offering more floor space, it would have required lowering the cabin floor to maintain sufficient headroom, thereby eliminating the critical under-floor volume needed for electrical wiring and other systems. A simple rectangular cabin layout was also evaluated but ultimately rejected due to the requirement for substantially stronger and thus heavier materials needed to maintain full atmospheric pressurization, which is regarded as essential for patient well-being.

3.3 Initial Sizing

Initial Sizing is the first step in the aircraft design loop. A suitable wing loading and Power-to-Weight ratio are set according to Raymer [75]. The main constraints are the Take-Off (T/O) and Landing Distance and the Climb with One Engine Inoperative (OEI). The Landing Distance is dependent on the Wing Loading, $C_{L,max}$ and the air density. Equation 1 from Raymer [75] is used to empirically estimate the maximum Wing Loading to achieve a landing distance of $s_{landing} = 756$ m.

$$(\mathrm{W/S}) = \frac{(s_{landing} - s_{safety}) \cdot \rho_{landing} \cdot C_{L,max}}{5 \cdot \rho_{Sea}} \cdot \ \mathrm{kg/m^3} \tag{1}$$

Assuming a $C_{L,max}$ of 3.5 a value of 325 kg/m^2 is calculated. This value is comparable to the wing loading of similar existing aircraft such as the ATR 72-500, which has (W/S) of 361 kg/m^2 [11].

The Power-to-Weight ratio depends on $C_{L,T/O}$ as well as the wing loading and the air density. Using equations by Raymer[75] and an assumed $C_{L,T/O}$ value of 2.5, a value of 0.21 W/N for (P/W) is calculated.

The final step of the Initial Sizing is the weight estimation. In order to proceed with the design loop, an initial maximum take-off mass must be estimated. This is done by estimating the empty mass fraction and the fuel fraction during the longest mission. The empty weight fraction is set to 0.55 and the fuel fraction is estimated to be 0.227 [75]. An estimated value of 3,600 kg for the payload including medical equipment onboard is chosen 3.1. Using calculations by Raymer [75], a value of 16,143 kg is chosen as the initial maximum take-off mass.

Figure 3 shows the design space and design point of ASCLERA for the initial sizing.

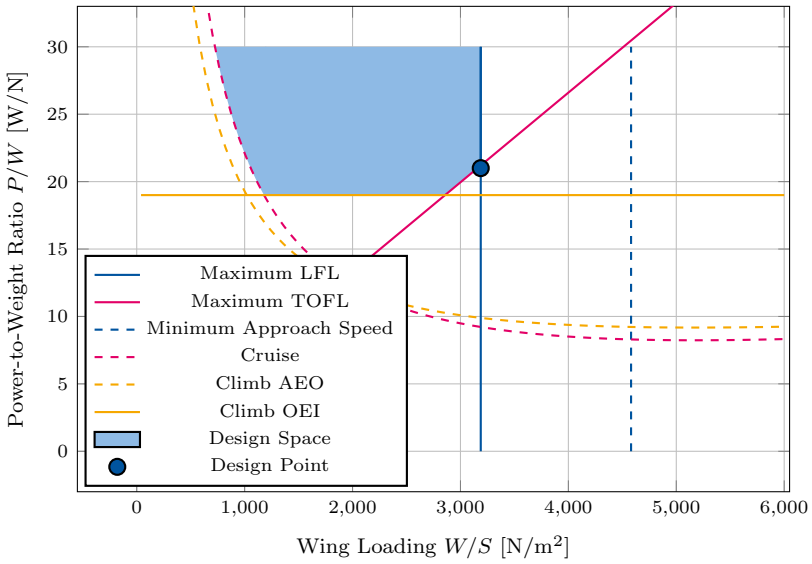

Figure 3: Design space and design point for ASCLERA.

4 Design Loop

Based on the initial design derived in section 3 a design loop is constructed. In this section the tools used (4.1), the implementation of the design loop (4.2), the tasks of the engineer in the loop (4.3) and decisions made prior to running the optimization (4.4) will be discussed.

4.1 Tools

To achieve a converged MTOM first of all an estimation method for the mass of different components of the aircraft is necessary. This is done on the basis of empirical formulas discussed by Raymer [75]. To function in an iterative setting, these methods are implemented within the developed Preliminary Design Tool. This tool is capable of calculating an MTOM based on the previous iterations value, the TLARs 1.3, further assumptions rooted in the given task and the fuel mass. The Flight Planning and Fuel Management (FPFM) Manual method by the International Civil Aviation (ICAO) Organization was used to calculate the fuel mass, which requires the lift-to-drag ratio (L/D) and the Power Specific Fuel Consumption (PSFC) [50, 90]. The PSFC is determined by scaling the PW127XT engine by γ_{rubber} so that it satisfies the thrust requirement and adding a safety factor of $\gamma_{safety} = 1.2$. The (L/D) is computed using calculatePolar, which is introduced in subsection 2.3. While it was also considered using VSPAERO [64] for aerodynamic calculations, this was not practical due to limitations in computing power and the inability to integrate the calculations into the design loop. A Matrix Laboratory (MATLAB) [86] script is coupling the Preliminary Design Tool and calculatePolar, which makes MATLAB the core program in this design loop. It is in charge of translating data between the different formats used in the Preliminary Design Tool and calculatePolar and controls the parameters of the loop and its convergence.

To validate the developed tool chain, a comparison was drawn between similar existing aircraft and the resulting aircraft. This includes geometry parameters, but focuses on the Operating Empty Mass (OEM) and MTOM. Due to assumptions for technology and materials with a time frame up to 2035, the achieved MTOM reduction of 27.5 % is within the expected range.

4.2 The Loop

In Figure 4 the different entities involved in the optimization loop and their tasks are depicted. The overall loop and an autonomous loop can be defined. The first involves the engineer in the loop and the second is shown as a loop in Figure 4 and only includes the Tools explained in subsection 4.1.

The initial weight estimation summarized in subsection 3.3 is used to set the starting value of MTOM_0.
For the current design an aerodynamic analysis using calculatePolar is carried out, driven by data the MATLAB code reads from the Preliminary Design Tool and writes into the corresponding input file for calculatePolar.

The MATLAB code then reads in the required data from the calculatePolar results and performs calculations to derive the $(\text{L/D})_{cruise}$ necessary for the mission analysis in the Preliminary Design Tool. To calculate $(\text{L/D})_{cruise}$ the lift coefficient

$$C_L = \frac{2 \cdot mg}{\rho_{cruise} \cdot Ma_{cruise}^2 \kappa R T_{cruise} \cdot S_{ref}} \tag{2}$$

is derived from a the force equilibrium $L = W$, where L is lift and W is the gravitational force. The density of the inflowing air at cruising altitude ρ_{cruise} and its Temperature T_{cruise} is determined using the International Standard Atmosphere (ISA) and the reference wing area S_{ref} is read from the Preliminary Design Tool. Additionally, the cruising Mach number M_{cruise} and the constants for the gravitational acceleration g, isentropic expansion factor κ and the specific gas constant R of air are used.

The (L/D) is calculated for the reference operating point top of climb (TOC) and top of descent (TOD) with the assumptions $m_{TOC} = \text{MTOM} - m_{taxi,dep} - 0.15 \cdot m_{TF}$ and $m_{TOD} = \text{MTOM} - m_{taxi,dep} - 0.97 \cdot m_{TF}$ respectively. $m_{taxi,dep}$ is the fuel mass needed for taxiing at the departure airport and m_{TF} is the trip fuel mass. For $(L/D)_{cruise}$ the mean value of both operating points is used. As mentioned in subsection 4.1, the Preliminary Design Tool is then used to calculate the new MTOM_n approximation based of the previous iteration MTOM_{n-1}, where n denotes the iteration step count. If this autonomous loop continues, the new design created by the Preliminary Design Tool will be sent to calculatePolar again. Further calculations of the static margin and T/O- and landing distances after the described autonomous loop ends are necessary as an input for the engineer in the loop (cf. subsection 4.3).

As a convergence criterion, the change of mass compared to the previous iteration is used (Δm). This value should be $\Delta\text{MTOM}_n = |\text{MTOM}_n - \text{MTOM}_{n-1}| < 0.03 \cdot \text{MTOM}_{n-1}$. The maximum allowable difference of 3 % is chosen, since

this lies within the expected error range of this method. Additionally, it was observed that for specific initial values of the optimization ΔMTOM_n was not strictly monotonically decreasing. Hence, the condition must be true for three consecutive iterations for convergence to be achieved.

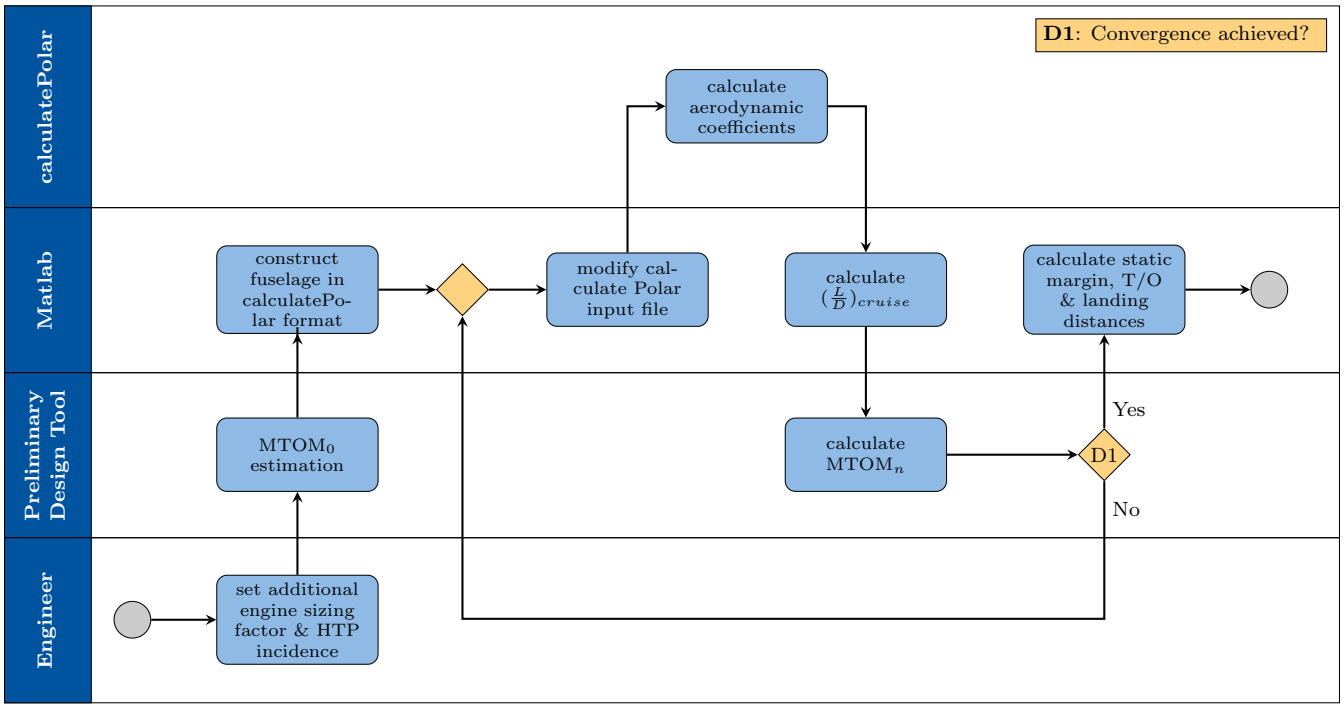

Figure 4: Swimlane diagram of the design loop.

Figure 5 illustrates the convergence of the mass for the final design. In this case the engineer in the loop sets the two free variables to their final values used for ASCLERA. Therefore, this figure does not show the iterative process of the whole design loop, but just the automated part. The starting value is the initial mass $\text{MTOM}_0 = 16,143$ kg (cf. subsection 3.3). After six iteration steps a mass of $\text{MTOM}_6 = 11,703$ kg has been reached, which is a reduction of 27.5 % from the initial estimate. The strictly monotone convergence displayed is the result of the simplifying assumption used in the Preliminary Design Tool.

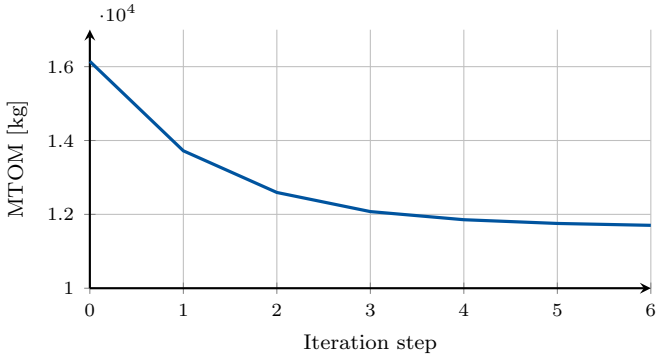

Figure 5: Weight progression in the design loop.

4.3 Engineer in the Loop

In addition to the tools listed in subsection 4.1, an engineer is necessary for a proper convergence of the design loop. The task of the engineer is to define the incidence of the horizontal tailplane (HTP) and an additional engine scaling factor from the outset of the automated optimization.

Since the basic aircraft geometry was fixed early into the design process, the wing position and fuselage length where unavailable variables for longitudinal stability. Furthermore, the position of the center of gravity (CG) is set by the geometry in cooperation with the payload placement. Hence, the HTP incidence was decided to be the only free variable for to achieve longitudinal stability. As a quantifiable measure of longitudinal stability the static margin is

$$SM \equiv \frac{x_{AC} - x_{CG}}{MAC} \cdot 100\% = -\frac{\partial C_M}{\partial C_L} \cdot 100\% \tag{3}$$

considered. x_{AC} and x_{CG} are the position of the aerodynamic center (AC) and the center of gravity along the longitudinal axis. MAC is the mean aerodynamic chord and c_m is the pitching moment coefficient. Typically a SM of 10 % is desirable for transport aircraft [75, p. 593]. Resulting from the approach taken to a modular cabin layout (cf. 5.1.4), the CG can be expected to move further forward for missions (cf. subsubsection 5.1.4), which are not covered in this report. Therefore a conservative value of $SM = 10$ % is the target for the design. To add further adaptability in the cabin layout and keep the CG position constant in flight a trim tank at the rear of the aircraft is used. Nevertheless, the target of $SM = 10$ % should still be aimed for in case of a reference cabin layout, since the trim tank has a limited authority on the CG position.

Figure 6: Position of the center of gravity and the aerodynamic center.

While the required power can be calculated using the statistical method by Raymer [75] using the T/O distance presented in 3.3, the distance for ASCLERA is near the boundary of the available values in this correlation [75]. Hence, a higher error in the (P/W) can be expected. To combat this, an additional calculation of the critical distance is performed. For ASCLERA, this distance refers to the required continued T/O distance following an engine failure at the decision speed V_1, which is then multiplied by a safety factor of 1.2. The engineer in the loop (see 4.3) is responsible to check the calculated distance of the design after the autonomous design loop has converged and adapt the additional engine scaling factor $\gamma_{additional}$ accordingly. $\gamma_{additional}$ is multiplied to the rubber engine factors γ_{rubber} and γ_{safety} described in subsection 4.1. The final design has an additional engine scaling factor of $\gamma_{additional} = 1.5$, which leads to a (P/W) of 0.38 W/N compared to (P/W) = 0.21 W/N in subsection 3.3.

Although it would have been possible to reduce the $\gamma_{additional}$ with a lower wing loading (see Equation 2), this would have resulted in a $C_{L,cruise}$ decrease and therefore a lower (L/D) during cruise.

4.4 Design Decisions

While implementing the design loop, design decisions were made that impacted the convergence behavior and the final result of the aircraft.

First of all, the use of the engineer in the loop instead of a fully autonomous loop has to be discussed. The computational time of one to three minutes for the automated part with the available system was typical for most design scenarios. Hence, the implementation of an optimizer for both variables in subsection 4.3 is omitted, as it is deemed to be too time intensive.

Second, the calculated (L/D) is adapted to translate the aircraft analyzed by calculatePolar to the one used in the design loop. To reduce complexity in the input file and the calculation using calculatePolar, the analyzed aircraft had no winglets. In line with Niranjanan [68] a (L/D) improvement of 8 % due to winglets is assumed.

Additionally, the lifting body capabilities of the elliptical fuselage are not taken into account in calculatePolar and are added retrospectively. According to subsection 2.2, an elliptic fuselage with ASCLERA's dimensions increases (L/D) by 20 %, when taking into account the correction factor of 1.043. The discussed drag reduction of the overall design will not be explicitly implemented, since this should occur during the design loop.

5 ASCLERA - Detailed Aircraft and Systems Design

In this section, the results of the design loop are explained in detail. The discussion will be divided into cabin and aircraft design. First, the cabin design 5.1 will be discussed, which led to the cabin and fuselage dimensions. Afterwards, the components of the aircraft will be introduced 5.2.

5.1 Cabin

The cabin is designed to directly implement the configuration selected in Section 3.2, which prioritized patient comfort, operational flexibility, and the need for a modular medical environment. The following sections detail how the chosen conventional airframe with an elliptical fuselage is realized to meet the specific mission TLARs, while keeping the cabin as small as possible and as spacious as necessary.

In order to achieve an optimized and balanced cabin, design choices are kept close to proven real-life standards and norms. Regarding workspace requirements for personnel and easy-access storage for medical equipment a paramedic as well as an Air Ambulance helicopter pilot were consulted to obtain real-life estimations and advice.

5.1.1 Cabin Dimensions and Features

As established in Section 3.2, a more conventional elliptical tube and wing fuselage with a width of 3.48 m and a height of 2.5 m was chosen. The cabin occupies the central 7 m of the fuselage, minimizing the impact of tapering at both the front and rear. By raising the floor 50 cm above the fuselage's lowest point, optimal headroom is provided particularly in walkable zones while maximizing usable surface area for seating and patient care. This elevated floor also accommodates substantial electrical wiring and utility routing beneath the cabin, enabling a clean and unobstructed interior layout. The electricity generated by the auxiliary power unit (APU) (cf. subsubsection 5.2.4) is sufficient to power all of the important medical equipment as well as the vital cabin features. To ensure patient needs are met in various ambient conditions, the system utilizes a climate control unit driven by the APU.

A two-door configuration is implemented. The addition of more doors would reduce usable interior space, while a single-door design would limit the ability to separate severely injured patients from others. This separation is considered critical in achieving the target turnaround time of ten minutes.

The aircraft is equipped with a large, upward-opening cargo door measuring 2.4 meters in width and 1.9 meters in height, allowing for an efficient boarding workflow, which is vital for MedEvac operations [48]. To handle critically injured patients, particularly in remote regions without proper infrastructure, an automated patient hoist is integrated directly into the large aft door.

When the door is opened, the APU-powered hoist is deployed downward. A stretcher is secured beneath the door and then lifted vertically above cabin floor height. From there, the hoist assembly moves horizontally along tracks mounted on the cabin ceiling. Once the Stretcher is transferred into the main cabin it is carried to its station by medical personnel, ensuring a swift and low strain transfer. For boarding lower acuity patients, the separate forward door is equipped with built-in stairs, comparable to those on a business jet.

A windowless cabin design is chosen to enhance structural performance, reducing vibration and cabin noise [66]. However, the lack of an external view may cause passenger disorientation. To mitigate this, large digital displays will be installed to provide a virtual window experience and alleviate potential discomfort. The net effect of replacing traditional windows with this system results in a weight reduction, which is detailed in Section 5.2.8.

5.1.2 Medical Care Standards

Acuity levels and the corresponding equipment and accommodations are first defined so that a cabin which can facilitate multi-acuity care may be designed. The acuity levels described by the Task are aligned with the Triage categories (SK) as defined by the Federal Office for Civil Protection and Disaster Relief [13]. In turn, different German ambulance types are aligned in their descriptions of care-capability with these SK levels. For instance, advanced life support for high acuity SK1 patients is provided by the Krankenkraftwagen Type C, or Rettungswagen (RTW, engl.: Mobile intensive care unit); basic emergency treatment and monitoring for medium acuity SK2 patients is provided by the Krankenkraftwagen Type B, or Notfallkrankenwagen (N-KTW, engl.: Emergency ambulance); and non-emergency transport for low acuity SK3 patients is performed by the Krankenkraftwagen des Type A, or Krankentransportwagen (KTW, engl.: Patient transport ambulance) [22, 29]. Hence, the underlying standard for equipment and medical loadout is adapted and adopted for this reason.

Equipment

The defined equipment loadouts in the key categories for immobilization, ventilation/respiration, diagnostics, infusion, managing life-threatening problems, bandaging and nursing aids, and personal protective equipment are adopted within the defined care standards from the European standard DIN EN 1789: "Medical vehicles and their equipment - Road ambulances" [22]. For trauma-specific missions, this baseline is augmented with advanced hemorrhage control capabilities, as detailed in Section 5.1.4.

Advanced Diagnostics

Following best practices in advanced pre-hospital and critical care, the baseline diagnostic suite defined in DIN EN 1789 [22] is supplemented with several point-of-care technologies to enhance diagnostic accuracy and enable goal-directed therapy. The deployment of these technologies is tiered to match patient acuity levels. Within the Diagnostics category, Point-of-Care Ultrasound (POCUS) is a versatile tool used for rapid triage and assessment in medium acuity patients and for comprehensive ongoing monitoring in high acuity trauma and cardiac arrest scenarios [94]. It is complemented by Non-invasive Electrical Cardiometry (EC), which provides continuous hemodynamic data essential for managing shock in SK1 patients [83]. Point-of-Care (POC) Blood Analysis is also added, contributing to both the Diagnostics and Infusion categories by providing critical data for metabolic and fluid management that informs interventions for both SK1 and SK2 patients [72]. Finally, Electrical Impedance Tomography (EIT) is included under the Ventilation/Respiration category for advanced, real-time lung monitoring [79], a capability reserved primarily for the most complex, mechanically ventilated SK1 patients. The integration of these systems elevates the standard of in-flight care from stabilization to data-driven, individualized intervention.

Medication

Under this standard, medication formularies are intentionally left to national regulations. Therefore, a practical basis for the medical supplies must be established. For this reason, the comprehensive medication list from the Rhein-Kreis Neuss (RKN) emergency service is used as a reference [10]. As no specific list for Type B (N-KTW) vehicles (which align with SK2 care) is provided, a suitable standard is derived from the RKN's RTW-backpack list. This list is comprised of all Type A (KTW) medication and a subset of essential, time-critical medications from the Type C (RTW) loadout. As such, an appropriate baseline for medications is established for SK2 patients, whose needs are positioned between SK3 and SK1.

Accommodations

Before summarizing the standards, the specific accommodations for each acuity level are detailed to clarify how patient needs are met and access by medical personnel is ensured.

- **SK3 (Low Acuity)** patients are accommodated in standard, forward-facing aircraft seats, as their condition requires minimal in-flight medical intervention beyond basic first aid.
- **SK2 (Medium Acuity)** patients are provided with half-reclinable, "business-class" style seats. This design offers enhanced comfort and allows medical staff better access for monitoring and basic interventions. The medical equipment to support these patients is provided via the Point-of-Use Mounting strategy, as detailed in Section 5.1.3.
- **SK1 (High Acuity)** patients require intensive, uninterrupted care and are therefore placed on a stretcher mounted on a Patient Transport Unit (PTU), similar in concept to the version used by the German Bundeswehr [49]. This unit is fully supported by both the Integrated Storage and Point-of-Use Mounting systems, as detailed in Section 5.1.3.

Furthermore, all patient accommodations are mounted on vibration-dampened fixtures to enhance patient comfort, a critical consideration during for take of from rough terrain and long duration flights. To ensure crew stability during turbulence, all patient accommodations are equipped with integrated grab handles, allowing for uninterrupted care.

This tiered framework is summarized in Table 4 below.

SK1 (High Acuity)	SK2 (Medium Acuity)	SK3 (Low Acuity)
Patient Accommodation		
Stretcher on a Storage Unit, similar to the Bundeswehr PTU [49]	Half-reclinable, "business-class" style seat.	Standard, forward-facing aircraft seat.
Equipment (DIN EN 1789) [22]		
Type C	**Type B**	**Type A2**
Medication List (RKN Table) [10]		
RTW & RTW-backpack	**RTW-backpack**	**KTW**

Table 4: Medical standards and accommodations by patient acuity level.

5.1.3 Medical Systems Implementation

With the individual patient requirements established, the overall cabin is designed as an integrated system to support simultaneous multi-acuity care. The core principle is to create an efficient workflow that allows medical personnel to manage multiple patients with varying needs without compromising care quality. This is achieved through a strategic layout combining patient blocks, a centralized medical workstation, and a tiered storage system.

Patient Grouping and Placement

To create an efficient workflow, patient accommodations are strategically placed according to their required level of care and access. SK3 patients, who require minimal medical access, are grouped into blocks (rows with 2 or 3 seats) in the forward section of the cabin. This allows for a more dense seating arrangement. Direct accessibility is ensured for both SK1 and SK2 patients through their placement. However, priority is given to SK1 patients, whose accommodations are positioned closer to workstations and, space permitting, are allotted a larger area.

The Medical Workstation

A dedicated medical workstation serves as the primary hub for the medical crew. Each medical drop-seat features a fold-down table for preparing interventions and a dedicated mounting system for a portable emergency kit including portable medical equipment compliant with DIN 13232; Emergency equipment [23] and medicine compliant with the RKN RTW-List [10]. This integrated setup enables the rapid and safe preparation of all necessary medications for SK1 and SK2 patients, with supplies easily replenished from the central storage area. The placement shown in Fig. 7 is designed to minimize the distance any patient has to the nearest workstation, ensuring interventions can be prepared and administered at a speed dictated by clinical urgency. For crew safety and stability during turbulent flight phases, the workstations and adjacent structures are also fitted with grab handles.

These tiered patient accommodations, along with drop-down seats are shown in Figure 7.

Figure 7: Interior of the cabin.

Telemedicine and AI-Assisted Monitoring

To leverage the telemedicine capabilities, the cabin is equipped with a sophisticated, multi-camera system. These cameras provide multiple high-resolution video feeds of the cabin, which can be securely transmitted to on-ground medical specialists for real-time remote consultation, alongside vital data streams from the advanced diagnostic tools

detailed in Section 5.1.2. Furthermore, this combined visual and diagnostic data stream enables an AI-based monitoring system designed to detect early signs of patient deterioration, such as changes in breathing patterns or signs of distress, acting as a force multiplier for the onboard crew and enhancing overall situational awareness.

Storage and Mounting Systems

A tiered storage strategy is implemented to ensure that medical equipment is available based on clinical urgency. The PTU for SK1 patients features Integrated Storage, a compartment below the stretcher housing all essential equipment for immediate intervention.

This is supplemented by the Point-of-Use Mounting system, which consists of flexible mounting points such as wall clips, seat attachments, and ceiling-mounted systems. This system is utilized for both SK1 and SK2 patients. For SK1 patients, relevant life monitoring systems are pre-deployed on these mounts as a baseline of care. For SK2 patients, the mounting points are used reactively to attach equipment for escalated care, such as infusion systems or the advanced diagnostic tools listed in Section 5.1.2 above.

Both systems are supplied by a modular Central Storage unit located at the rear of the cabin, which holds bulk supplies, SK3 equipment, and refills for all kits and medications, ensuring efficient supply management for the entire mission.

5.1.4 Rapid Reconfiguration and Modularity

The ability to rapidly switch between mission profiles is achieved through two key technical systems that allow for maximum interchangeability.

To minimize turnaround times, a fully automated rail system is employed for loading and unloading all patient accommodation modules (SK1 PTUs, SK2 seats, and SK3 seats) through the rear cargo door. Tracks integrated into the cabin floor are equipped with an automated transport mechanism, which comprises rotating cylinders within the rails and conical elements at crossings, a design inspired by Disney's Infinite Treadmill concept. The track layout is strategically designed to keep the area in front of the aft door unobstructed, preserving essential access for onboarding high acuity patients on stretchers. A floor plan of this layout and a potential use case are shown in Figures 8 and 9.

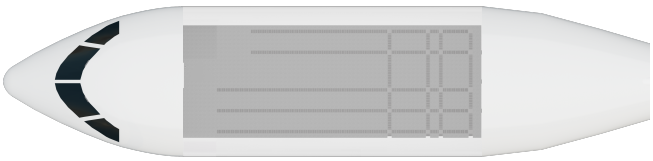

Figure 8: ASCLERA's in-floor rail system.

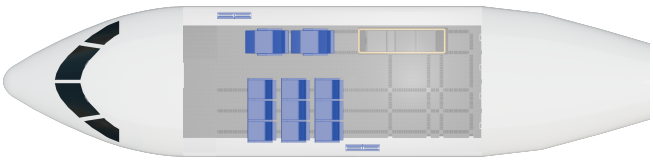

Figure 9: ASCLERA's mission equipment.

Cones are selected over more conventional spherical elements due to spatial constraints. A classical solution using spheres would either require diameters too large for the track width or, if smaller, would necessitate a greater number of elements, resulting in excessive mechanical complexity for two-dimensional movement. Cones mitigate this issue by requiring only one actuator per cone to be implemented in the floor. To minimize the use of the APU all systems can be powered through on-base facilities.

To prevent obstruction of personnel or passengers during flight, a simple roller cover for the longitudinal tracks is implemented. This cover is stored in the tail section of the aircraft and can be extended as needed. As the cover can only be deployed from the rear, all loading operations are inherently configured to proceed from front to back. No longitudinal track remains accessible between seats due to the length of the seat base structures.

In configurations involving multiple PTUs or a combination of PTUs and seats, the PTUs are equipped on both sides with manually deployable rubber flaps to facilitate smooth transitions. For the lateral tracks, simple metal covers are used, stored adjacent to each rail within the cabin floor.

Using this system, the aircraft can be rapidly and efficiently reconfigured for specific mission profiles by ground crews. This modular approach is based on established practices in both military and civilian aviation, where rapid-change systems and modularity are commonly employed to maximize operational flexibility [31].

As mentioned in 5.1.3 a highly Modular Central Storage System is utilized. Highly modularized compartments compose this central storage area at the back of the cabin. Entire compartments are quickly swapped out, enabling rapid restocking. Individual drawers and containers are standardized, allowing medical supplies to be easily grabbed by personnel and taken to their workstation for efficient kit refilling.

All ground handling procedures, including the use of ground support equipment (GSE) and cabin reconfiguration, are made to comply with the operator's manuals and industry good practices, ensuring that the aircraft is operated and maintained using existing airport infrastructure and logistics chains.

The combination of the automated rail system and modular storage units provides significant operational flexibility. The payload budget, established from the mass breakdown in subsection 3.1, is shown to effectively accommodate the comprehensive care standards defined for the aircraft. The primary design case, Mission 2, requires transport of 15 patients, 4 medics, 2 pilots, and 500 kg of cargo, which fits comfortably within the 3,600 kg payload capacity at a required mission range of 800 km (see Figure 11). Furthermore, the system's adaptability is demonstrated by its ability to handle two theoretical maximums: a max acuity configuration with 3 SK1 patients and 6 medical staff, and a max-density configuration for 20 SK3 patients with 4 medical staff. Considering the mass budgets, both scenarios are validated to be within the payload limits, confirming that ASCLERA possesses the payload capacity for a wide range of operational needs.

Beyond defined mission profiles, the core strength of the ASCLERA platform is its "plug-and-play" adaptability. The modular architecture of the cabin and the strategic use of the central storage unit are designed to accommodate mission-specific equipment packages that go far beyond the advanced baseline suite. This includes dedicated modules for proven specialized missions like transporting patients on extracorporeal membrane oxygenation (ECMO) or infant transport decks with incubators [85]. Furthermore, the system is designed to incorporate emerging, state-of-the-art capabilities for trauma care, such as a portable blood cooler for Low Titer O Whole Blood transfusion and the equipment for in-flight Resuscitative Endovascular Balloon Occlusion of the Aorta (REBOA) [74, 78]. The viability of performing such a delicate vascular procedure is directly enabled by the aircraft's stable flight environment, which is a result of the advanced flight control system and gust load alleviation system detailed in 5.2.7. This adaptability ensures ASCLERA can be quickly tailored to meet the unique clinical demands of any complex patient transfer.

5.2 Aircraft

This subsection covers the technical data of ASCLERA. It details individual components as well as mass and performance metrics. Figure 10 shows the three-sided view of ASLCERA, including dimensions and ground clearance angles. An overview of the aircraft data is given in Table 5.

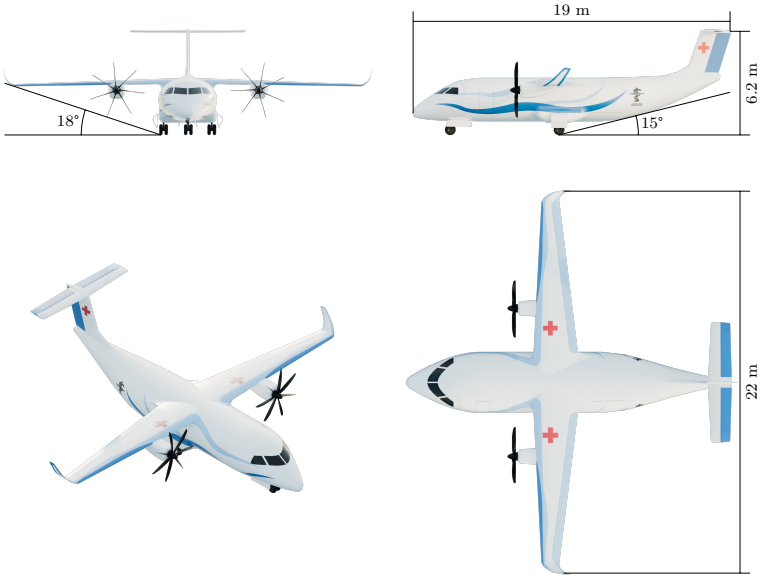

Figure 10: Three sided view of the aircraft.

Aircraft Data	
Length	19 m
Height	6.2 m
TOFL	749 m
LFL	714 m
Wingspan	22 m
Aspect Ratio	13
Taper Ratio	0.45
φ_{LE}	3 °
MAC	1.748 m
$(t/c)_{max,root}$	17 %
$(t/c)_{max,tip}$	13 %
Fuselage Height	2.6 m
Fuselage Width	3.5 m
OEM	6,398 kg
MTOM	11,703 kg
MZFM	9,998 kg
Cruise Speed	Ma 0.4
Cruise Altitude	FL200

Table 5: Specifications of the aircraft, wing and performance.

5.2.1 Final Mass and Aircraft Performance

Using the design loop described in section 4 the final MTOM of the aircraft is determined. The mass breakdown of the individual components is presented in Table 6.

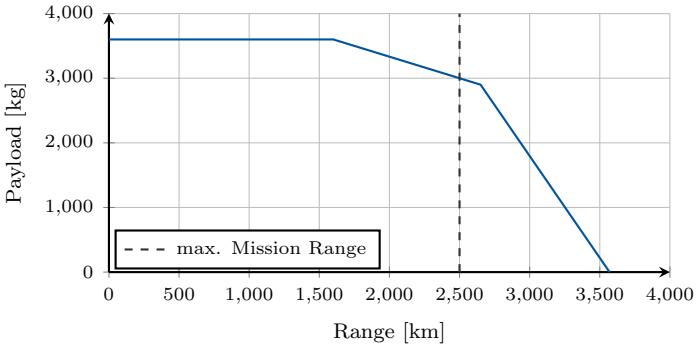

Figure 11: Payload-Range diagram of ASCLERA.

Component Masses	
Wing	461 kg
HTP	81 kg
VTP	80 kg
Fuselage	2,731 kg
Nose LG	89 kg
Main LG	499 kg
Engine	1,076 kg
All Else Empty	1,381 kg
Payload	3,600 kg
Fuel	1,705 kg
Total	**11,703 kg**

Table 6: Specifications of the aircraft masses.

The payload-range diagram of ASCLERA is shown in Figure 11. It was created considering a time to climb and a reserve holding time of 30 min each, a design fuel mass of 1,705 kg and a maximum fuel mass of 2,400 kg. The design range is 2,500 km, based on the longest mission M3. As observable, this range condition is met while transporting 3,000 kg of payload. Since mission 3 represents an extreme case in terms of mission radius (see Table 1), it is not flown with the full payload. The selected design point therefore ensures sufficient range to cover all three mission scenarios. It does not lie at the top-right corner of the diagram, as it results from a trade-off between multiple mission requirements and includes safety margins, rather than maximizing range or payload individually.

Figure 7 lists aerodynamic properties of ASCLERA. While $C_{L,opt}$ is significantly higher than $C_{L,cruise}$ the $(\mathrm{L/D})_{cruise}$ is just 7.7 % reduced compared to the optimum. Furthermore it should be noted, that the wave drag $C_{D,wav}$ represents a drag fraction of 0.6 %. This is due to the cruising Mach number being in the compressible, but not yet transonic regime.

The static margin of $SM = 10$ % was achieved in the final design as set out to be in subsection 4.3. As stated in subsection 3.2 a pitch angle of $\Theta = 0$ ° is desirable for patient comfort. This goal has been achieved within an acceptable range during cruise with $\alpha_{cruise} = -0.2906$ °.

Aerodynamic data	
Re_{cruise}	$9.1 \cdot 10^6$
$C_{L,cruise}$	0.58
$C_{L,opt}$	0.88
α_{cruise}	−0.29 °
$C_{D,cruise}$	0.0260
$C_{D,ind}$	0.0103
$C_{D,wav}$	0.0001
$C_{D,visc}$	0.0156
$(\mathrm{L/D})_{cruise}$	22.30
$(\mathrm{L/D})_{opt}$	24.63
SM	10 %

Table 7: Aerodynamic data and drag component breakdown.

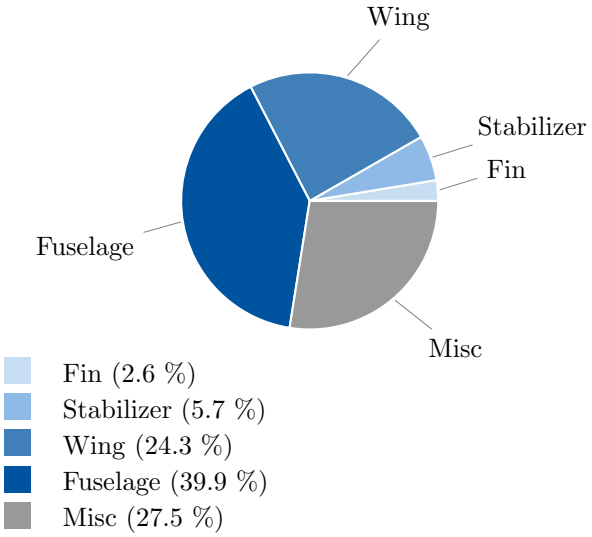

Figure 12: Drag breakdown into aircraft components.

5.2.2 Landing Gear

The position of the landing gear strongly influences the balance of the aircraft during ground operations. With the CG known, the nose and main landing gear are positioned and the track width is chosen so that the longitudinal and lateral tip-over criteria are met [90]. During this process, the static loads are distributed between main and nose landing gear according to the design rules of Raymer [75]. Furthermore, sufficient ground clearance is factored in and the resulting configuration is checked for lateral ground clearance. This reduces the risk of a tail strike and allows a possible roll angle during landing.

5.2.3 Wing

The wings planform is derived from the wing loading (W/S) = 325 kg/m^2 determined in subsection 3.3 the MTOM of the current iteration, which is 11,703 kg for the final design (see Table 6), the aspect ratio Λ and taper ratio λ.

The taper ratio $\lambda = 0.45$ is fixed during iterations, as this leads to minimal induced drag for an untwisted wing [80]. $\Lambda = 13$ has been assumed fixed as well.

This value is above most turboprop aircraft compared by Marinus et al. [61], but only marginally higher than the aspect ratio of the de Havilland Canada DHC-8 Series 100 and the proposal of Nicolosi et al., whose values are $\Lambda = 12.43$ and $\Lambda = 12$ respectively. The coefficient $\frac{k_{engine}}{k_{engine}-1} \frac{\text{MTOM}}{P_{shaft}} \sqrt{\frac{\text{MTOM}}{S_{ref}}}$ used by Marinus et al. [61] is computed to about 90 for both the DHC-8 and ASCLERA, where k_{engine} is the engine number and P_{shaft} the maximum shaft power, which makes this a suitable comparison. The DHC-8 had its maiden flight in 1983, while the proposed aircraft is designed for Entry into Service in 2035. Therefore, assuming $\Lambda = 13$ is plausible for a 2035 technology level, especially considering that both compared aircraft have a longer wingspan, thus alleviating some of the material challenges due to a lower root bending moment. [70, 67]

Although natural laminar flow airfoils as well as hybrid laminar flow control have potential to reduce drag, this can only be achieved if the surface stays free from contamination or damage during operations [90]. As presented in Table 3 ASCLERA shall be able to operate in a wide range of conditions, which includes unpaved runways. Particularly in combination with the whirl up of reverse thrust, the requirement of contamination free surfaces can not be guaranteed. Hence, further consideration of laminar flow is omitted. Additionally, a morphing wing concept was considered. While this could improve aerodynamic efficiency, Dong [25] indicates that a weight penalty has to be implemented, which would reduce ASCLERAs STOL capabilities. Furthermore, the high technical complexity and resulting reliability concerns render the morphing wing unfeasible for the given missions [25].

Oriented on the Saab 340, which uses the National Aeronautics and Space Administration (NASA) developed MS(1)-0316 at the root and MS(1)-0312 at the tip, ASCLERA uses NASA MS(1)-0317 (see Figure 14) at the root and MS(1)-0313 (see Figure 13) at the tip. Since these airfoils are used in a similar operational scenario and publicly available they where deemed suitable for this design. The differing thickness between the inner and outer airfoil was chosen to provide enough structural rigidity, especially considering the comparably high aspect ratio and therefore high wing root bending moment. [54, 77]

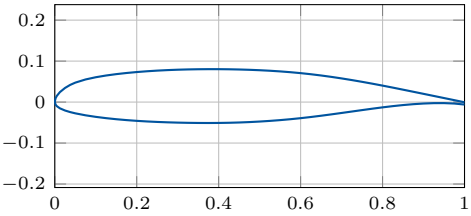

Figure 13: Inner airfoil of ASCLERA: NASA MS(1)-0313.

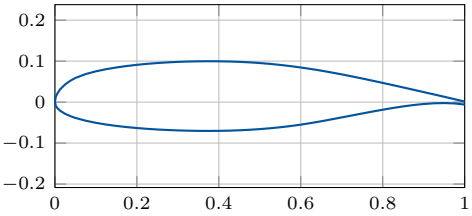

Figure 14: Outer airfoil of ASCLERA: NASA MS(1)-0317.

5.2.4 Propulsion

The propulsion system is designed by calculating the required power and scaling an existing turboprop engine as described in 4.3. The Pratt & Whitney PW127XT was chosen to power ASCLERA, since its power does not require excessive engine scaling and performance data is publicly available [32]. Additionally, it is capable of operating on SAF, which part of the TLARs (cf. subsection 3.2). Today's regularities only allow a SAF mix of up to 50 % but until 2030 Airbus expects to be able to run on 100 % SAF [8]. It is the successor to the PW127 and improved the power specific fuel consumption by 3 %, while keeping the same dimensions. The total engine power is calculated by the engineer in the loop using equation 4.

$$P_{total} = \gamma_{rubber} \cdot \gamma_{safety} \cdot \gamma_{additional} \cdot (\mathrm{P/W})_{initial} \cdot \mathrm{MTOM} \tag{4}$$

The final maximum engine data is given by Table 8 [40, 71, 73]. On the ground, an APU powers the electrical systems of the aircraft.

Powertrain Data	
Engine Length	2,316 mm
Engine Diameter	783 mm
Engine Mass	1,076 kg
PSFC	$7.517 \cdot 10^{-8}$ g/Ws
Prop Diameter	2,925 mm
$k_{blade,prop}$	7
γ_{rubber}	0.906
γ_{safety}	1.2
$\gamma_{additional}$	1.5
P_{shaft}	4025 kW

Table 8: Specifications of the powertrain.

5.2.5 Empennages

Due to the high wing configuration of the aircraft, a T-tail configuration was chosen for the tail in order to maintain elevator control at high angles of attack. To design the empennages, the volumetric coefficient method as described by Raymer [75] is used. This method can be applied to estimate the area of the tail plane that is required to maintain control and stability without complex calculations during the design loop. It factors in the wing reference area S_{ref}, the MAC, the volumetric coefficients v_{HTP} and v_{VTP}, and the respective moment arms r_{HTP} and r_{VTP}. As a conservative method of estimating, one can assume that the resulting areas of the horizontal and vertical tail plane are sufficient. The airfoil used for the empennages is shown in Figure 15.

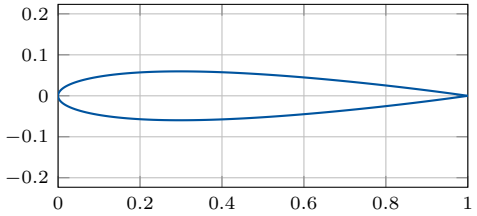

Figure 15: Empennage airfoil of ASCLERA: NACA 0012.

Horizontal tail plane

The formula to calculate the horizontal tail plane is given below [75].

$$S_{HTP} = \frac{v_{HTP} \cdot S_{ref} \cdot MAC}{r_{HTP}} \tag{5}$$

The volumetric coefficient v_{HTP} is assumed to be 0.95 [75]. The area of the HTP is calculated to be 6.32 m^2.

Vertical tail plane

The vertical tail plane is calculated using the following equation [75]:

$$S_{VTP} = \frac{v_{VTP} \cdot S_{ref} \cdot b_W}{r_{VTP}} \tag{6}$$

With an assumed volumetric coefficient v_{VTP} of 0.076, the area of the VTP is calculated to be 6.27 m^2.

5.2.6 High Lift Systems

The design of the high lift system is critical to achieve the necessary STOL capabilities. The trailing edge flap system consists of an oscillating advanced dropped hinged flap. This system works by rotating a single flap around a dropped hinge at the trailing edge of the wing. The resulting slit at the top of the trailing edge is closed by the spoilers deflecting downwards [89]. Compared to Fowler flaps, a higher flap deflection angle can be achieved, further increasing the maximum Lift Coefficient. The flap system can be used during cruise flight for further advanced load alleviation, increasing patient comfort in turbulent conditions. Reduced technical complexity compared to slotted fowler flaps reduces weight as well as maintenance requirements. The trailing edge flap system paired with a leading edge slat system to increase the critical angle of attack of the wing.

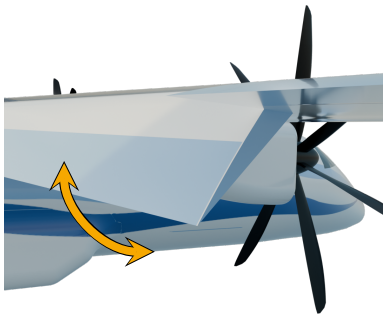

Figure 16: Flap oscillating around $\alpha_{flap,crit}$.

In landing configuration, the trailing edge flaps are extended and oscillate around their critical angle of attack. Studies show that this can increase the critical angle of attack of the flap and thus increase $C_{L,max}$ by delaying the detachment of the airflow [76]. Initial numerical studies show an increase in the Lift coefficient by 3% in landing configuration. The analyses are carried out on an advanced dropped hinged flap system. A maximum Lift Coefficient of 3.2 is achieved on a 3D wind tunnel model [76]. An additional Lift gain due to propeller wash and the resulting increase in local air speed is considered, therefore a maximum Lift Coefficient of 3.5 can be assumed in combination with a leading edge slat system instead of a simple droop nose system. It must be noted that his system must be closely controlled by the fly-by-wire computers to maintain stability during high lift conditions. After touchdown the flaps are extended further to an angle of 80° to increase drag and stall the flap system. The spoilers deflect upwards to increase drag further and increase the friction between the tyres and the ground. This decreases the landing distances and reduces brake temperatures to allow for a fast turnaround.

During take-off, the high lift system partially deflects to induce a $C_{L,T/O}$ of 2.5. To further minimize the take off distance, the flaps are extended just before reaching the decision speed V_1. This reduces drag during the take-off roll. Another benefit is that it increases ground controllability by reducing the lift, therefore increasing the friction between the ground and the tires.

5.2.7 Flight Control System

ASCLERA, in accordance with its TLARs (cf. subsection 1.3), incorporates a fly-by-wire system, to improve the safety of the aircraft and to be able to include Control Laws [15]. These Control Laws are inspired by the ones used by Airbus [6]. Although degraded Control Laws are considered, in this report just the Normal Law will be discussed. The systems described below allow for a reduction in the pilots workload, which can improve safety especially in regions where the pilot needs to allocate a lot of his capacity to navigating difficult terrain, like in mission 1 (see Table 1). To further assist the pilot, haptic feedback is provided to mimic manual controls.

Aircraft Behavior

Along the pitch axis ASCLERA will follow the C* control law. This combines the load factor n_z at the pilots seat and the pitch rate q, to achieve an intuitive control of the aircraft.
Commanding a turn, the pilot controls the roll rate p. The turn coordination and compensation provides the required rudder and elevator deflection for a level turn with no slip angle β.
The input to control surface allocation is not fixed. Depending on the state and configuration, a multi-use control surface approach is taken.
The pitch and roll rates are limited to $q = 3\ °/s$ and $p = 15\ °/s$ respectively to improve patient comfort. These values simulate the behavior required by the Airbus Standard Operating Procedures (SOP) [6, 5], which is used for larger and less agile aircraft than ASCLERA. The pilot is able to switch into a higher agility mode within the Normal Law with the flip of a switch to not compromise on safety in mountainous regions.

Flight Envelope Protection

The flight envelope protections (FEP) allow the aircraft to be safely operated within its whole flight envelope, without the risk of a stall of damage to the structure. Being capable of flying at the maximum climb angle without the risk of stall is crucial for safe operations in mission 1.
In line with Airbus, the following FEP are used in the Normal Law:

- Pitch Attitude Protection
- Load Factor Limitation
- High Speed Protection
- High Angle of Attack Protection
- Bank Angle Protection

The High Angle of Attack Protection and High Speed Protection, while adapted this design case, are not changed in their functionality. The Pitch Angle Protection for ASCLERA is modified to be separated into two pitch angle Θ regimes. For up to $\Theta_{prot,up} = 15\ ^\circ$ nose up and $\Theta_{prot,down} = 10\ ^\circ$ nose down the pilot controls the aircraft via the C* control law as discussed above. Exceeding Θ_{prot} the pilots sticks deflection responds linearly to the pitch angle with a maximum at $\Theta_{max,up} = 30\ ^\circ$ in case of nose up and $\Theta_{max,down} = 15\ ^\circ$ for nose down.
This functionality is already included in the Bank Angle Protection by Airbus, but $\Phi_{prot} = 20\ ^\circ$ is a reduced value compared to the Airbus A320. Φ_{max} is set to 67 °.
Furthermore, the Load Factor Limitation is modified. It still limits the load factor to $-1 \leq n_z \leq +2.5$, in line with the CS-25 [30]. But it is expanded to increase the input force required to operate outside of $+0.5 \leq n_z \leq +1.5$. These values are picked, because the variation from +1 lies within the mean peak of patient transport as discussed by Silbergleit et al. [82]. This force feedback approach is similar to the one taken by Boeing [52], but this implementation is done to not interfere with Pitch Attitude Protection and still has a hard limit on the load factor.
These changes are made to reduce ASCLERAs typical operating flight envelope in the name of patient comfort and, in the case of the Load Factor Limitation, to not disrupt the functionality of medical equipment. It hast to be noted, that it is still possible to use the whole flight envelope in case it is necessary for safe operations.

Gust Load Alleviation

During cruise flight, the trailing edge flap systems (cf. 5.2.6) can be used to alleviate gust loads and therefore increase the patient's comfort due to the reduction of turbulence effects. As stated in subsection 3.2, this is seen as a priority in the design process. Due to the low cruise altitude, turbulence due to weather must be expected. Therefore, systems must be in place to reduce the risk of injuring patients and medical personnel onboard. An advanced laser turbulence detection system paired with a high performance weather radar installed in the nosecone detects turbulence up to 75 m ahead of the aircraft [91]. The flight control computers process the information and calculate the necessary flight control deflection. At a cruising speed of Mach 0.4 at an altitude of 20,000 ft, this gives the aircraft approximately 0.5 s to move the control surfaces. In addition to the conventional control surfaces, the oscillating flap system can also be used to temporarily increase or decrease drag and lift during gusts due to its faster response time compared to conventional flap systems.

5.2.8 Fuselage

As discussed in subsection 5.1, the cabin is pressurized to atmospheric pressure at sea level for patient safety and comfort. This leads to strong pressure differences at cruise altitude and results in stresses on the fuselage structure. In a cylindrical fuselage, only normal circumferential stresses occur due to pressurization. With increasing eccentricity, an elliptic fuselage experiences additional bending loads. To bear these extra loads, further structural supports have to be considered. Following the approach of Boulle [14], which was introduced in subsection 2.2, the eccentricity of the fuselage is used to determine the volume penalty of the elliptical fuselage. Considering an unsymmetrical sandwich construction with a thick core for the fuselage shell, the structural volume increases by 80 % compared to a circular fuselage made from the same material. The use of carbon-fiber-reinforced plastics (CFRP) in a composite fuselage structure results in a decrease in density of the shell of 55.6 % compared to aluminum. These effects compensate each other, that is, the weight increase due to eccentricity is offset by the weight reduction achieved through the use of lightweight materials.

The windowless fuselage design, which was introduced in subsection 5.1, combines multiple advantages. It increases the fatigue strength of the fuselage, reduces noise inside the cabin, reduces maintenance costs, and allows for easier manufacturing. In addition, replacing windows with digital displays results in a weight reduction of 0.5 % of the overall aircraft [66].

The rear fuselage tapers over a length of 7 m from the full cross-section to the tail. Due to the fuselage being wider than it is tall, there is a potential risk of flow separation in the tail area, which would cause additional drag. To mitigate this, the aft section of the fuselage is aerodynamically shaped. Furthermore, vortex generators are installed on the rear fuselage surface, following Raymer's approach [75], which was introduced in subsection 2.2.

6 Mission Analysis

This section details ASCLERAs operations, starting with first response (6.1), followed by the turnaround process (6.2). Finally mission execution (6.3) compares the timeframe given in subsection 3.1 with the capabilities of the final design.

6.1 First Response

Upon mission reception, a two-minute window is dedicated to initial preparations, this time is utilized to contact doctors and pilots and to calculate the mission requirements.

Based on these requirements, a scalable loadout strategy is employed to stock the Central Storage unit mentioned in 5.1, optimizing for both unit-based consumables (e.g., breathing masks) and rate-based consumables (e.g., oxygen) to tailor weight and redundancy for each flight.

After this calculation window, the physical preparation of the aircraft commences, beginning with the configuration of the cabin according to the selected loadout. This loading process, which proceeds from front to back, is the most time-consuming phase of the first response, as patient accommodation modules like PTUs and seats must be loaded sequentially due to spatial constraints at the door. The Gantt chart shown below in Figure 17 illustrates an exemplary scenario for this process. This phase also includes pre-loading essential equipment onto the point-of-use mounting points (see Section 5.1.3) to ensure immediate readiness upon arrival.

While the cabin is being configured, the aircraft is fueled according to the mission profile. The configuration process has an upper time limit of 20 minutes, though this can be reduced to as little as five minutes if the system is not configured to full capacity.

Once loading and fueling are complete, the aircraft is checked for readiness. After verification, the boarding bridges are retracted, and the aircraft is prepared for take-off.

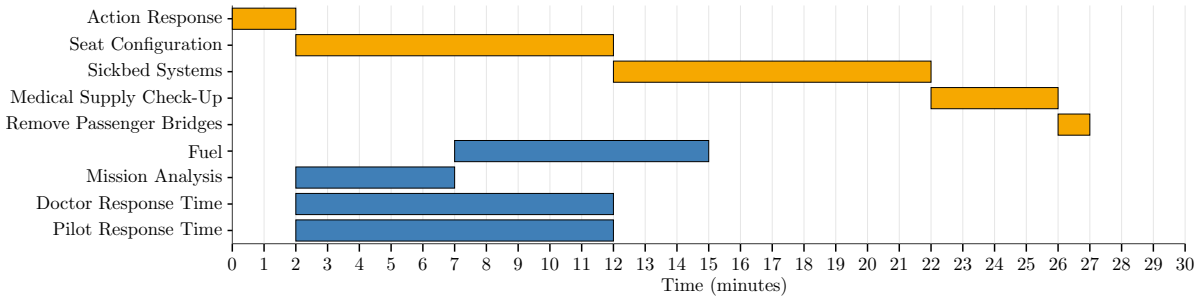

Figure 17: First response process for ASCLERA.

6.2 Turnaround Process

Upon landing at the destination, the aircraft doors open, and medical personnel immediately begin triage on the ground, utilizing equipment such as POCUS as discussed in Section 5.1.2 for rapid assessment. Physically impaired patients are supported by medical staff.

Based on this initial assessment, a dual boarding process begins, utilizing both the forward and aft doors simultaneously to segregate patient flows by acuity. While SK2 and SK3 patients board through the forward door via its integrated stariway, the rear door is dedicated to high-acuity SK1 patients. As dictated by the on-site triage, the required number of stretchers are lowered from the aircraft for these patients. After transfer, each occupied stretcher is raised by the integrated winch into the cabin as discussed in section 5.1.1.

This dual-door approach is key to efficient patient handling, and its flexibility is demonstrated by the different time allocations across various scenarios. The five-minute passenger boarding time illustrated in the Gantt chart (Figure 18) corresponds to the maximum passenger scenario mentioned in Sec. (subsubsection 5.1.4) with only SK3 patients, where a streamlined process is ensured by the medical crew. In contrast, for Mission 1, the 10-minute turnaround time is deliberately used to allow for extensive on-site triage and initial stabilization of the high-acuity patient. For the high-volume Mission 2, the 10-minute turnaround is allocated for rapid triage of all 15 patients to efficiently manage the parallel boarding flow.

For highly specialized critical care missions, such as Mission 3, the turnaround time is highly dependent on the complexity of the patient's condition and the required equipment. Onboarding a patient who requires life-support systems like an ECMO machine involves a more intricate process of securing both the patient and the equipment, which can extend the turnaround time from the baseline of 7 minutes up to 25 minutes.

Simultaneously to patient boarding, the cargo compartment can be cleared if required by the mission profile, independent of the onboarding process. This further enhances operational flexibility and the range of mission types the aircraft can fulfill.

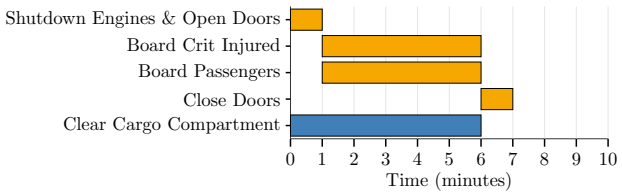

Figure 18: Turnaround process for ASCLERA.

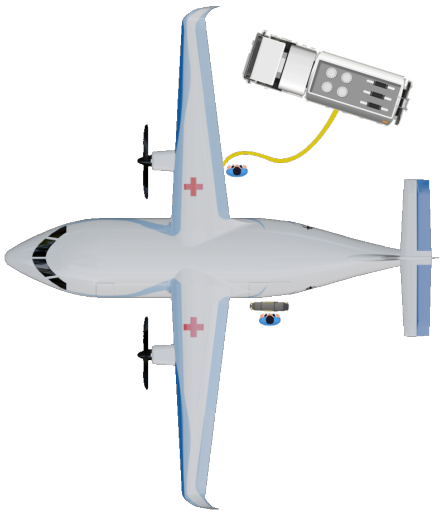

Figure 19: Top view of ASCLERA during simultaneous refueling and patient handover.

The aircraft's wingspan of 22 m and MTOM of 11,703 kg place it within the range of small to medium-sized aircraft, which are regularly accommodated at regional airports using standard GSE and handling infrastructure. These airports are equipped to handle aircraft of this size with existing taxiways, stands, and aprons, as well as conventional refueling vehicles and hydrant systems, since the fuel capacity of 2,000 kg is well within the operational range of standard refueling equipment. The height of 3.41 meters and landing gear height of 0.86 meters allow the use of typical passenger stairs, medical lifts, and loaders, as these are designed for a variety of aircraft dimensions within this category [34]. The twin turboprop configuration is also common among regional aircraft, ensuring that maintenance personnel, spare parts, and servicing procedures are widely available at most airports. Ground handling service providers must adapt their procedures and equipment to match the specific geometry and medical use case of the aircraft, ensuring both technical compatibility and patient safety. This is illustrated schematically in figure 19, which shows the coordinated refueling and patient transfer operations around the ASCLERA platform [31].

6.3 Mission Execution

The final Mission Execution shows significant improvements compared to the assumptions in the Initial Design phase. While staying at a cruise speed of Mach 0.4 time is saved due to fast responses and quick turnaround, listed in Table 9 for the cases displayed in the Gantt charts. This would allow for slower flight times, increasing $(L/D)_{cruise}$. But since the airplane is designed in a medical context, in which transport times are critical, the theoretically slower flight speeds are not considered further. Additionally, it allows for unplanned delays when navigating mountains or specific airspaces, helping to guarantee fast and reliable patient transports. The take-off and landing distances shown are the minimum achievable distances when using maximum take-off power and full braking. During mission execution, lower power and brake settings can be used to reduce acceleration, especially on longer runways. In the critical design case of an engine failure at V_1, a T/O distance of 749 m is achieved, including the obstacle hight of 15 m.

Parameter	Mission 1 *Remote Response*	Mission 2 *Disaster Response*	Mission 3 *Critical Transfer*
Mission Time			
Response Time [min]	27	27	15
One Way Flight Time [min]	25	58	158
Turnaround [min]	7	7	7
Total Time [min]	83	151	339
Take-Off and Landing at Pick-Up location			
Takeoff distance (m)	548	284	322
Landing distance (m)	569	380	420
Equipment and Mission Window			
Cabin Layout	2×SK1 1×2×SK2 1×3×SK3	4×1×SK2 4×3×SK3	1×SK1
Time saved compared to mission window [min]	7	59	201

Table 9: Specification of the mission execution for the three individual missions.

7 Discussion and Outlook

This section discusses the key technologies used for ASCLERA in subsection 7.1 and provides an overview of possible future developments in medical evacuation in subsection 7.2.

7.1 Key Technologies for ASCLERA

The Technology Readyness Level, which was introduced in subsection 2.4, is used to assess the key technologies of ASCLERA regarding a possible EIS after 2035. All relevant key technologies listed in Table 10 have at least been validated in a laboratory environment (TRL 4), with the exception of the oscillating flap system, which has only been validated analytically [76]. This allows for the assumption that all these technologies will be ready for EIS around 2035. Composite wing and empennage structures are already being used in today's aircraft, for example in the B787 [39] and A350 [7]. Artificial windows have already been installed in some of Emriates' B777 airplanes [12]. All other technologies are in different phases of development. The Clean Sky 2 project [19] has produced the Multi Function Fuselage Demonstrator (MFFD), a four diameter fuselage structure made from composite materials. Smaller diameter composite fuselages are already being used in today's aircraft, e.g. in the HondaJet [38]. NASA's D8 transport configuration, which incorporates a lifting body fuselage, has been evaluated in a low speed wind tunnel. AI-assisted monitoring of patients has already been used for specific cases of trauma care, e.g. for sepsis prediction for ICU patients [84] and trauma tracking and alerting [20], demonstrating that it is functional in a relevant environment. With regard to the automatic loading of the aircraft, multiple existing technologies will be combined. This includes an in-floor rail system [42], the automatic installation of equipment similar to [35] and scaled-down automated guided vehicles (AGV) similar to [59].

Key Technology	TRL	Source
Composite Structure Fuselage	5/9	[19, 21, 36, 38]
Composite Structure Wings and Empennage	9	[39, 7]
Lifting Body Fuselage	4	[27]
Windowless Fuselage	9	[12]
Oscillating hinged flap	3	[76]
AI-Assisted Monitoring	6	[20, 84]
Automatic loading of aircraft	4-5	[35, 41]
Advanced Gust Detection and Load alleviation	7	[91]

Table 10: TRL for key technologies of ASCLERA.

7.2 Future Developments

Future developments of the ASCLERA concept focus on enhancing autonomy, mission adaptability, and environmental sustainability. Building upon the existing modular cabin and automated loading systems, several key areas for innovation have been identified:

The automation of turnaround procedures is a major objective, including robotic systems for cabin cleaning, disinfection, and restocking of medical supplies. Concepts such as self-disinfecting surfaces and autonomous replenishment systems are being investigated to reduce human error and optimize operational efficiency, especially in time-critical scenarios [31].

Future iterations of the modular rail system aim to enable dynamic cabin reconfiguration during flight. Adaptive actuators and smart locking mechanisms could allow transitions between mission profiles (e.g. from high-density evacuation to intensive care transport) in response to real-time medical assessments. Preliminary research indicates feasibility under moderate structural and safety constraints [42].

Algorithms trained on historical mission data offer the potential to enhance mission preparation and support in-flight decision-making. By analyzing patterns in patient conditions, logistical constraints, and operational parameters, such systems can propose optimized cabin configurations, supply loads, and treatment workflows in real time. Preliminary studies in the context of MedEvac operations indicate that data-driven support tools can contribute to reduced response times and improved quality of care [69].

The transition towards "more electric aircraft" promotes the use of compact, lightweight actuators such as piezoelectric or magnetostrictive systems. These technologies enable faster, quieter, and more reliable cabin adjustments with reduced mass and energy demand, essential for in-flight reconfigurability and fine-tuned equipment control [18].

Even though environmental compatibility is not a top priority, significant long-term reductions in emissions are expected from hydrogen-electric and hybrid propulsion systems. Projects like Airbus ZEROe and demonstrators from ZeroAvia aim to mature these technologies towards commercial viability by the 2040s. However, current challenges in hydrogen storage and refueling infrastructure remain critical for remote operations [4, 47].

Infrastructure-wise, compatibility with decentralized SAF supply chains or mobile hydrogen refueling units is essential for MedEvac deployment in remote or disaster-prone areas to extend range.

To enhance the range of medical scenarios ASCLERA can address, the integration of a mobile surgical unit may be considered. Similar concepts have been realized by Johnson Medical, which developed mobile operating rooms for deployment in war zones and disaster relief settings [65]. Given ASCLERA's modular rail infrastructure, the incorporation of such capabilities appears technically feasible and could significantly extend the platform's operational versatility.

8 Evaluation and Conclusion

In this section, first, ASCLERA's design is evaluated in subsection 8.1, then subsection 8.2 concludes this report.

8.1 Fulfillment of the Design Specifications

The final ASCLERA design is evaluated with a focus on the achieved TLARs of this year's Design Challenge. Table 11 lists the compliance of the proposed concept with the TLARs defined in subsection 1.3. The overall compliance with the TLARs is summarized here, further details on individual TLAR fulfillment are provided in sections 5 and 6.

ID	TLARs ASCLERA	TLAR Compliance
1	Simultaneous Multi-Acuity Care	achieved
2	Rapid Mission Reconfiguration	achieved
3	STOL capabilities on unpaved runways	achieved
4	Range and operational radius	achieved
5	Cabin adaptability and patient throughput	achieved
6	Payload capacity of 3,600 kg	achieved
7	Flight level 200 and $Ma_{cruise} = 0.4$	achieved
8	Advanced fly-by-wire systems and control laws	to be verified in flight tests

Table 11: Overview of the achieved TLARs.

8.2 Conclusion

The design process of ASCLERA presented in this work demonstrates that a carefully balanced integration of modular medical equipment, advanced flight systems, and a novel yet partially conventional airframe architecture can meet the complex requirements of post-2035 aeromedical missions. By aligning the aircraft's capabilities with stringent mission-specific TLARs - such as simultaneous multi-acuity care, rapid reconfigurability, STOL performance at high elevations, and a range of 2,500 km - the resulting design achieves high operational versatility, patient safety, and logistical efficiency.

A central element in achieving the ASCLERA design was the structured and iterative design loop, which systematically refined the configuration based on mission-specific requirements and aerodynamic performance. Supported by UNICADO's calculatePolar tool, the loop enabled the convergence of the MTOM while incorporating key innovations across the aircraft architecture. These include the elliptic lifting-body fuselage for increased internal volume and aerodynamic efficiency, oscillating flaps to enhance STOL performance, and a modular rail-based system for flexible and automated patient loading. The resulting aircraft configuration satisfies all critical TLARs, including the ability to transport up to 15 patients and 6 crew members, operate from 756 m unpaved runways at 2,850 m elevation, and cover mission ranges of up to 2,500 km.

With regard to technological feasibility, the assessment of key systems indicates that most are already in use or in advanced stages of development, with demonstrated potential for readiness around 2035. While some innovative components - such as the oscillating flap system-are still in earlier stages, the majority of ASCLERA's technologies are based on established or actively maturing solutions. This supports the credibility of the proposed EIS timeframe and reduces risks in development.

Taken together, ASCLERA offers a pragmatic, future-ready and operationally adaptable solution for aeromedical evacuation beyond 2035. It not only addresses current MedEvac challenges but also lays a foundation for future advancements in modularity, automation, and sustainable aviation technologies.

References

[1] ADAC: 50 Jahre ADAC Ambulanz-Service: Uns schickt der Himmel, https://www.adac.de/der-adac/ueber-uns-se/ambulanceservice/geschichte/ (accessed 07/02/2025).

[2] ADAC: Die eigene Flotte des ADAC Ambulanz-Service — ADAC, https://www.adac.de/der-adac/ueber-uns-se/ambulanceservice/transportmoeglichkeiten/flotte/ (accessed 07/02/2025).

[3] ADAC: Unsere Hubschrauber - ADAC Luftrettung, https://luftrettung.adac.de/hubschrauber/ (accessed 07/02/2025).

[4] Airbus S.A.S: ZEROe: our hydrogen-powered aircraft, https://www.airbus.com/en/innovation/energy-transition/hydrogen/zeroe-our-hydrogen-powered-aircraft (accessed 07/11/2025).

[5] Airbus S.A.S.: A focus on the takeoff rotation, https://safetyfirst.airbus.com/a-focus-on-the-take-off-rotation/ (accessed 07/19/2025), 2021.

[6] Airbus S.A.S.: A319/320 FCOM DSC - Aircraft Systems - Part 2, Aug. 3, 2012.

[7] Airbus S.A.S.: Airbus technical magazine - Special Edition A350XWB, 2013.

[8] Airbus S.A.S.: Airbus' commitment to sustainable aviation fuel, https://www.airbus.com/en/innovation/energy-transition/our-commitment-to-saf (accessed 07/11/2025).

[9] Airport Technology: Eurocopter EC 145, https://www.airport-technology.com/projects/eurocopter_ec145/?cf-view (accessed 07/11/2025).

[10] ÄLRD Rhein Kries Neuss: Einheitliche Medikamentenliste RKN Stand August 2024, 2024-06-30.

[11] ATR Aircraft: ATR 72-500, https://www.atr-aircraft.com/wp-content/uploads/2020/07/72-500.pdf (accessed 07/15/2025).

[12] BBC: Emirates looks to windowless planes, 2018.

[13] Bevölkerungsschutz und Katastrophenhilfe, B. für: Triage - Sichtung, https://www.bbk.bund.de/DE/Themen/Gesundheitlicher-Bevoelkerungsschutz/Triage-Sichtung (accessed 07/15/2025).

[14] Boulle, A.; Dubé, M.; Gosselin, F. P.: Parametric study of an elliptical fuselage made of a sandwich composite structure. Mechanics Research Communications, Vol. 69, pp. 129–135, 2015.

[15] Brockhaus, R.; Alles, W.; Luckner, R.: Flugregelung, Berlin, Heidelberg: Springer, ISBN 978-3-642-01442-0, 2011.

[16] Capt. Shervon Pope: Army paramedics shape future MEDEVAC aircraft design, https://www.army.mil/article/281837/army_paramedics_shape_future_medevac_aircraft_design (accessed 07/11/2025).

[17] Charter, G.: Differences between Air Ambulance, Medevac, and Casevac, https://www.globalcharter.com/de/post/differences-between-air-ambulance-medevac-and-casevac (accessed 07/14/2025).

[18] Claeyssen, F.; Grohmann, B.; Christmann, M.; Lorkowski, T.; Le Letty, R.: New Actuators for Aircraft and Space Application. Proc. 11th International Conference on New Actuators, Bremen, Jan. 2008.

[19] Clean Aviation Joint Undertaking: Clean Sky 2 achievement report – 2014 - 2024, a decade of innovation for a sustainable European aviation industry, Publications Office of the European Union, 2025.

[20] Croatti, A.; Montagna, S.; Ricci, A.; Gamberini, E.; Albarello, V.; Agnoletti, V.: BDI personal medical assistant agents: The case of trauma tracking and alerting. Artificial Intelligence in Medicine, Vol. 96, pp. 187–197, 2019.

[21] Deutsches Zentrum für Luft- und Raumfahrt: MFFD – using thermoplastics to replace aluminium in aircraft construction, https://www.dlr.de/en/latest/news/2023/03/mffd-thermoplastics-instead-of-aluminium-in-aircraft-construction (accessed 07/11/2025).

[22] DIN Deutsches Institut für Normung e.V: Medical vehicles and their equipment - Road ambulances; English version EN 1789:2020+A1:2023, English translation of DIN EN 1789:2024-07, 2024-07.

[23] DIN Deutsches Institut für Normung e.V: Notfall-Ausrüstung; DIN 13232:2011-05, 2011-05.

[24] Dolev, E.: The First Recorded Aeromedical Evacuation in the British Army – The True Story. BMJ Military Health, Vol. 132, No. 1, pp. 34–36, 1986.

[25] Dong, C.; Arief, M. M.: Morphing Wing Designs in Commercial Aviation. arXiv preprint arXiv:2502.07182, 2025.

[26] Dornier 328 Excecutive Specifications, Performance, and Range, https://www.globalair.com/aircraft-for-sale/specifications?specid=1230 (accessed 07/02/2025).

[27] Drela, M.: Development of the D8 Transport Configuration. In: 29th AIAA Applied Aerodynamics Conference. American Institute of Aeronautics and Astronautics, (cit. on pp. 4, 6, 23), 2011.

[28] DRF Stiftung Luftrettung gemeinnützige AG: Die Flotte der DRF Luftrettung, https://www.drf-luftrettung.de/luftrettung/flotte (accessed 07/18/2025).

[29] DRK Rettungsdienst Eifel-Mosel-Hunsrück gemeinnützige GmbH: Rettungsfahrzeuge, https://www.drk-emh.de/dienststellen/rettungsfahrzeuge/uebersicht.html (accessed 07/15/2025).

[30] European Aviation Safety Agency: CS-25 - Amendment 18, https://www.easa.europa.eu/en/downloads/21117/en (accessed 07/19/2025), June 22, 2016.

[31] European Aviation Safety Agency: Operational Requirements For Ground Handling Services (Part GH.OPS), https://www.easa.europa.eu/sites/default/files/dfu/annex_iv_gh.ops_operational_requirements_draft.docx_0.pdf (accessed 07/11/2025).

[32] European Aviation Safety Agency; Pratt & Whitney Canada: Type-Certificate Data Sheet PW100 series, IM.E.041, 2014.

[33] Federal Aviation Administration: Operational Priority for MEDEVAC Flights, https://www.faa.gov/documentLibrary/media/Notice/N_JO_7110.774_Operational_Priority_for_MEDEVAC_Flights.pdf (accessed 07/11/2025).

[34] Flughafen Zurich AG: Aircraft Ground Handling Emissions, https://www.flughafen-zuerich.ch/-/jssmedia/airport/portal/dokumente/das-unternehmen/politics-and-responsibility/environmental-protection/technische-berichte/2014_gse_emissionmeth_zrh.pdf?vs=1 (accessed 07/11/2025).

[35] Fraunhofer IFAM: Clean Sky 2 – ACCLAIM: Efficient installation of lighter sidewalls and hand luggage compartments through automation, https://www.ifam.fraunhofer.de/en/Press_Releases/acclaim.html (accessed 07/11/2025).

[36] Fraunhofer IWS: Laser Technology for a Lighter Future Flying - Fraunhofer IWS, https://www.iws.fraunhofer.de/en/newsandmedia/press_releases/2024/press-release_2024-05_CONTIjoin-ESL-BUSTI.html (accessed 07/11/2025).

[37] Frolov, V.: Optimization of Lift-Curve Slope for Wing-Fuselage Combination. In: Aerodynamics. Rijeka: IntechOpen, chap. 4, (cit. on p. 4), 2019.

[38] Fujino, M.: Case Study 4: HondaJet. In: Fundamentals of Aircraft and Airship Design: Volume 2 – Airship Design and Case Studies. American Institute of Aeronautics and Astronautics, pp. 615–647, ISBN 978-1-60086-898-6, (cit. on p. 23), 2013.

[39] Giurgiutiu, V.: Boeing 787 Dreamliner - an overview — ScienceDirect Topics, https://www.sciencedirect.com/topics/engineering/boeing-787-dreamliner (accessed 07/11/2025).

[40] Gudmundsson, S.: Chapter 7 - Selecting the Power Plant. In: General Aviation Aircraft Design. Boston: Butterworth-Heinemann, pp. 181–234, ISBN 978-0-12-397308-5, (cit. on p. 18), 2014.

[41] Hanna: Rail System For Seat Assembly In An Aircraft. Patent, US9868506B2, Jan. 2018.

[42] Hanna, Klaus and Bruno, Daniele and Kriewall, Rainer: Rail system for seat assembly in an aircraft, https://patents.google.com/patent/US9868506B2/en (accessed 07/11/2025).

[43] Harris, F. D.: Tiltrotor Conceptual Design, NASA/CR—2017–219474, Mar. 2017.

[44] Hefazi, H.; Vore, A.; Dougherty, D.: High lift flap design and testing for a tailless transport aircraft, Jan. 2013.

[45] Hoff, T.; Becker, F.; Dadashi, A.; Wicke, K.; Wende, G.: Implementation of Fuel Cells in Aviation from a Maintenance, Repair and Overhaul Perspective. Aerospace, Vol. 10, No. 1, 2023.

[46] Horstmann, K.-H.: Ein Mehrfach-Traglinienverfahren und seine Verwendung für Entwurf und Nachrechnung nichtplanarer Flügelanordnungen. PhD thesis, 1987.

[47] Houten, A. van: A No-Emissions Flight, https://time.com/7094860/zeroavia-za600/ (accessed 07/11/2025).

[48] IATA: IOSA Standards Manual, https://www.iata.org/contentassets/8658ac253f6848a79480a6da70c85d5f/iosa_standards_manualism_edition_12.pdf (accessed 07/11/2025).

[49] Ink, S.: Patiententransporteinheit – PTE, https://www.bundeswehr.de/de/organisation/luftwaffe/aktuelles/patiententransporteinheit-pte-246624 (accessed 06/15/2025).

[50] International Civil Aviation Organization: Flight Planning and Fuel Management (FPFM) Manual, Doc 9976, 2015.

[51] International Organization for Standardization: ISO 16290:2013: Space systems — Definition of the Technology Readiness Levels (TRLs) and their criteria of assessment, 2013.

[52] Kornecki, A.: Approaches to Assure Safety in Fly-by-Wire Systems: Airbus vs. Boeing. In: IASTED Conf. on Software Engineering and Applications, 2004.

[53] Kozuba, J.; Pila, J.; Martinec, F.: Analysis Of Possible Modification Of Transport Aicraft To Medevac In The Czech Republic. Scientific Journal of Silesian University of Technology. Series Transport, Vol. 118, pp. 109–121, Mar. 2023.

[54] Lednicer, D.: The Incomplete Guide to Airfoil Usage, https://m-selig.ae.illinois.edu/ads/aircraft.html (accessed 07/15/2025).

[55] Leonardo S.p.A.: Successfully performed the first ground run test of the NGCTR's Technology Demonstrator, https://www.leonardo.com/en/news-and-stories-detail/-/detail/ngctr-td-convertiplano-primo-test-messa-moto-a-terra (accessed 07/11/2025).

[56] Liebeck, R. H.: Design of the Blended Wing Body Subsonic Transport. Journal of Aircraft, Vol. 41, No. 1, pp. 10–25, 2004.

[57] Liersch, C.; Engelbrecht, T.: LIFTING_LINE: Ein Mehrfach-Traglinienverfahren für Entwurf und Nachrechnung nichtplanarer Flügelanordnungen, 2019.

[58] Lim, J. C.: The evolution of air ambulances through the decades, https://www.aerotime.aero/articles/31806-air-ambulance-evolution-through-decades (accessed 07/02/2025), 2022.

[59] Lödige Industries: Automated Guided Vehicles (AGV) for baggage and cargo ULDs, https://www.lodige.com/en-global/products/airport-logistics/air-freight-logistics/mobile-terminal-equipment/agv-automated-guided-vehicle/ (accessed 07/11/2025).

[60] Mankins, J.: Technology Readiness Level – A White Paper, Jan. 1995.

[61] Marinus, B. G.; Quodbach, L.: Data and Design Models for Civil Turbopropeller Aircraft. Journal of Aircraft, Vol. 57, No. 6, pp. 1252–1267, 2020.

[62] Massaro, M.; Biga, R.; Kolisnichenko, A.; Marocco, P.; Monteverde, A.; Santarelli, M.: Potential and technical challenges of on-board hydrogen storage technologies coupled with fuel cell systems for aircraft electrification. Journal of Power Sources, Vol. 555, p. 232397, Jan. 2023.

[63] May, M. S.; Milz, D.; Looye, G.: Transition Strategies for Tilt-Wing Aircraft. In: AIAA Scitech 2024 Forum. AIAA, (cit. on pp. 3, 6), 2024.

[64] McDonald, R. T.: OpenVSP (Open Vehicle Sketch Pad), 2019.

[65] Medical, J.: Mobile Surgical Unit, http://www.johnsonmedical.com/web/product.asp?sec=3&art=17 (accessed 07/15/2025).

[66] Moruzzi, M. C.; Bagassi, S.: Preliminary design of a short-medium range windowless aircraft. International Journal on Interactive Design and Manufacturing (IJIDeM), Vol. 14, No. 3, pp. 823–832, Sept. 2020.

[67] Nicolosi, F.; Corcione, S.; Trifari, V.; De Marco, A.: Design and Optimization of a Large Turboprop Aircraft. Aerospace, Vol. 8, No. 5, 2021.

[68] Niranjanan, C. K.; Arshad Shameem, C.; Shikhar Jaiswal, A.; Venkatesh, T. N.: Winglet Aerodynamic Optimization of a 19-Seater Turboprop Aircraft. In: Advances in Multidisciplinary Analysis and Optimization, Pradeep Pratapa, P.; Saravana Kumar, G.; Ramu, P.; Amit, R. K., 2023.

[69] OpenMedScience: How AI Is Improving Medevac Response Times and Patient Care, https://openmedscience.com/how-ai-is-improving-medevac-response-times-and-patient-care/ (accessed 07/11/2025).

[70] Palt, K.: de Havilland Canada / Bombardier DHC-8 Dash 8, https://www.flugzeuginfo.net/acdata_php/acdata_dhc8_en.php (accessed 07/15/2025), 2019.

[71] Perry, D.: ATR re-engines with new PW127XT series and secures launch order from Air Corsica — News — Flight Global. FlightGlobal, 2021.

[72] Plebani, M.; Nichols, J.; Luppa, P.; Greene, D.; Sciacovelli, L.; Shaw, J.; Khan, A.; Carraro, P.; Freckmann, G.; Dimech, W.; Zaninotto, M.; Spannagl, M.; Huggett, J.; Kost, G.; Trenti, T.; Padoan, A.; Thomas, A.; Banfi, G.; Lippi, G.: Point-of-care testing: state-of-the art and perspectives. Clinical Chemistry and Laboratory Medicine (CCLM), Vol. 63, pp. 35–51, June 2024.

[73] Pratt and Whitney: PW127XT, `https://www.prattwhitney.com/en/products/regional-aviation-engines/pw127xt` (accessed 07/16/2025).

[74] Rajesh, A.; Barry, L.; Giersch, C.; Danko MBE, K. L.; Bowers, A.; Braverman, M.; Epley, E.; Rose, T.; Whole Blood Consortium, S. A.; Bryan, Cotton; Brian, E.; Jenkins, D.: Prehospital Whole Blood Transfusion Improves Probability of Survival Over Transfusion Within One Hour of Arrival to a Trauma Center. The American Journal of Surgery, p. 116530, 2025.

[75] Raymer, D.: Aircraft Design: A Conceptual Approach, Sixth Edition, ISBN 978-1-62410-490-9, Sept. 2018.

[76] Ruhland, J.; Breitsamter, C.: Numerical analysis of high-lift configurations with oscillating flaps. CEAS Aeronautical Journal, 2021.

[77] Saab AB: Saab 340, `https://www.saab.com/products/saab-340` (accessed 07/15/2025).

[78] Sadek, S.; Lockey, D. J.; Lendrum, R. A.; Perkins, Z.; Price, J.; Davies, G. E.: Resuscitative endovascular balloon occlusion of the aorta (REBOA) in the pre-hospital setting: An additional resuscitation option for uncontrolled catastrophic haemorrhage. Resuscitation, Vol. 107, pp. 135–138, Oct. 2016.

[79] Scaramuzzo, G.; Pavlovsky, B.; Adler, A.; Baccinelli, W.; Bodor, D. L.; Damiani, L. F.; Franchineau, G.; Francovich, J.; Frerichs, I.; Giralt, J. A. S.; Grychtol, B.; He, H.; Katira, B. H.; Koopman, A. A.; Leonhardt, S.; Menga, L. S.; Mousa, A.; Pellegrini, M.; Piraino, T.; Priani, P.; Somhorst, P.; Spinelli, E.; Händel, C.; Suárez-Sipmann, F.; Wisse, J. J.; Becher, T.; Jonkman, A. H.: Electrical impedance tomography monitoring in adult ICU patients: state-of-the-art, recommendations for standardized acquisition, processing, and clinical use, and future directions. Critical Care, Vol. 28, No. 1, p. 377, Nov. 2024.

[80] Schlichting, H.; Truckenbrodt, E.: Aerodynamik des Flugzeuges: Aerodynamik des Tragflugels (Teil II), des Rumpfes, der Flugel-Rumpf-Anordnung und der Leitwerke. Klassiker der Technik, Springer Berlin, Heidelberg, ISBN 978-3-642-56910-4, 2001.

[81] Schültke, F.; Stumpf, E.: UNICADO: Aufbau und Etablierung einer universitären Flugzeugvorentwurfsumgebung, `https://publications.rwth-aachen.de/record/828728/files/828728.pdf`, 2021.

[82] Silbergleit, R.; Dedrick, D.; Pape, J.; Burney, R.: Forces acting during air and ground transport on patients stabilized by standard immobilization techniques. Annals of Emergency Medicine, Vol. 20, No. 8, pp. 875–877, Aug. 1991.

[83] Slagt, C.; Servaas, S.; Ketelaars, R.; Geffen, G.-J. van; Tacken, M. C. T.; Verrips, C. A.; Baggen, L. A. M.; Scheffer, G. J.; Eijk, L. T. van: Non-invasive electrical cardiometry cardiac output monitoring during prehospital helicopter emergency medical care: a feasibility study. Journal of Clinical Monitoring and Computing, Vol. 36, No. 2, pp. 363–370, Apr. 2022.

[84] Sun, B.; Lei, M.; Wang, L.; Wang, X.; Li, X.; Mao, Z.; Kang, H.; Liu, H.; Sun, S.; Zhou, F.: Prediction of sepsis among patients with major trauma using artificial intelligence: a multicenter validated cohort study. International Journal of Surgery, Vol. 111, No. 1, ID: 01279778-202501000-00042, 2025.

[85] Swiss Air-Ambulance Ltd: Leading expertise in complex patient transport, `https://www.swiss-air-ambulance.ch/special-missions` (accessed 07/09/2025).

[86] The MathWorks Inc.: MATLAB version: 25.1.0 (R2025a), 2025.

[87] Thomas, R. H.; Burley, C. L.; Nickol, C. L.: Assessment of the Noise Reduction Potential of Advanced Subsonic Transport Concepts for NASA's Environmentally Responsible Aviation Project. In: 54th AIAA Aerospace Sciences Meeting, (cit. on pp. 3, 6), 2016.

[88] U.S. Department of Energy: Hydrogen Storage — Department of Energy, `https://www.energy.gov/eere/fuelcells/hydrogen-storage` (accessed 07/09/2025).

[89] Univ.-Prof Dr.-Ing. E. Stumpf: Flugzeugbau 1, 2025.

[90] Univ.-Prof Dr.-Ing. E. Stumpf: Flugzeugbau 2, 2025.

[91] Univ.-Prof Dr.-Ing. E. Stumpf: Systeme der Luft- und Raumfahrt, 2025.

[92] Univ.-Prof Dr.-Ing. Peter Jeschke: Luftfahrtantriebe I und II, 2024.

[93] Universal Air Evac: Future Trends in the Air Ambulance Industry: A Convergence of Aviation and Healthcare, https://uniairevac.com/future-trends-air-ambulance-industry-convergence-aviation-and-healthcare (accessed 07/11/2025).

[94] Vianen, N. J.; Van Lieshout, E. M.; Vlasveld, K. H.; Maissan, I. M.; Gerritsen, P. C.; Den Hartog, D.; Verhofstad, M. H.; Van Vledder, M. G.: Impact of Point-of-Care Ultrasound on Prehospital Decision Making by HEMS Physicians in Critically Ill and Injured Patients: A Prospective Cohort Study. Prehospital and Disaster Medicine, Vol. 38, No. 4, pp. 444–449, 2023.

[95] Wiart, L.; Atinault, O.; Grenon, R.; Paluch, B.; Hue, D.: Development of NOVA Aircraft Configurations for Large Engine Integration Studies. In: 33rd AIAA Applied Aerodynamics Conference. AIAA, (cit. on p. 6), 2015.

[96] Wölcken et. al.: Smart intelligent aircraft structure, https://link.springer.com/book/10.1007/978-3-319-22413-8 (accessed 07/11/2025).

[97] Wolleswinkel, R. E.; Vries, R. de; Hoogreef, M.; Vos, R.: A New Perspective on Battery-Electric Aviation, Part I: Reassessment of Achievable Range. In: AIAA SCITECH 2024 Forum, (cit. on pp. 3, 6).

[98] Zimmnau, M.; Schültke, F.; Stumpf, E.: UNICADO: multidisciplinary analysis in conceptual aircraft design. CEAS Aeronautical Journal, Vol. 14, No. 1, pp. 75–89, 2022.